conventional diffractometers of that era. For accurate Rietveld modelling or accurate charge-density studies, the theoretical scattered intensity must be known. This is not a problem at synchrotron-radiation sources, where the incident beam is initially almost completely linearly polarized in the plane of the orbit, and is subsequently made more linearly polarized through Bragg reflection in the monochromator systems. Rather, it is a problem in the laboratory-based systems where the source is in general a source of elliptical polarization. It is essential to determine the polarization for the particular monochromator and the source combined to determine the correct form of the polarization factor to use in the formulae used to calculate scattered intensity (Chapter 6.2).

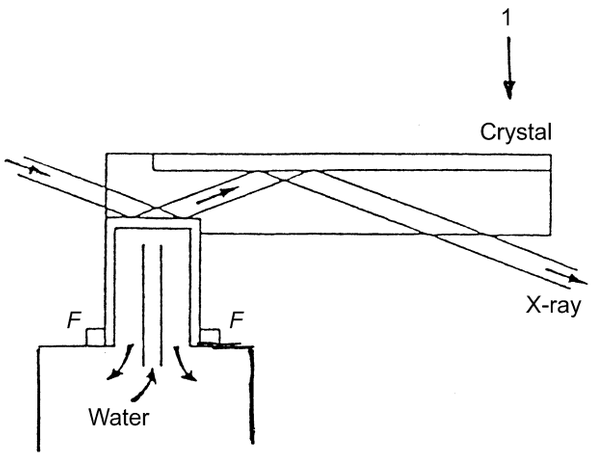

Fig. 4.2.5.6. A schematic diagram of a Hart-type tuneable channel-cut monochromator is shown. The monochromator is cut from a single piece of silicon. The reflecting surfaces lie parallel to the (111) planes. Cuts are made in the crystal block so as to form a lazy hinge, and the second wafer of the monochromator is able to be deflected by a force generated by a current in an electromagnet acting on an iron disc glued to the upper surface of the wafer. Cooling of the primary crystal of the monochromator is by a jet of water falling on the underside of the wafer. This type of system can tolerate incident-beam powers of 500 W mm^{-2} without significant change to the width of the reflectivity curve.

4.2.6. X-ray dispersion corrections (By D. C. Creagh)

The term 'anomalous dispersion' is often used in the literature. It has been dropped here because there is nothing 'anomalous' about these corrections. In fact, the scattering is totally predictable.

For many years after the theoretical prediction of the dispersion of X-rays by Waller (1928), and the application of this theory to the case of hydrogen-like atoms by Hönl (1933*a*,*b*), no real use was made by experimentalists of dispersion-correction effects in X-ray scattering experiments. The suggestion by Bijvoet, Peerdeman & Van Bommel (1951) that dispersion effects might be used to resolve the phase problem in the solution of crystal structures stimulated interest in the practical usefulness of this hitherto neglected aspect of the scattering of photons by atoms. In one of the first texts to discuss the problem, James (1955) collated experimental data and discussed both the classical and the non-relativistic theories of the anomalous scattering of X-rays. James's text remained the principal reference work until 1974, when an Inter-Congress Conference of the International Union of Crystallography dedicated to the discussion of the topic produced its proceedings (Ramaseshan & Abrahams, 1975).

At that conference, reference was made to a theoretical data set calculated by Cromer & Liberman (1970) using relativistic quantum mechanics. This data set was later used in *IT* IV (1974) and has been used extensively by crystallographers for more than a decade.

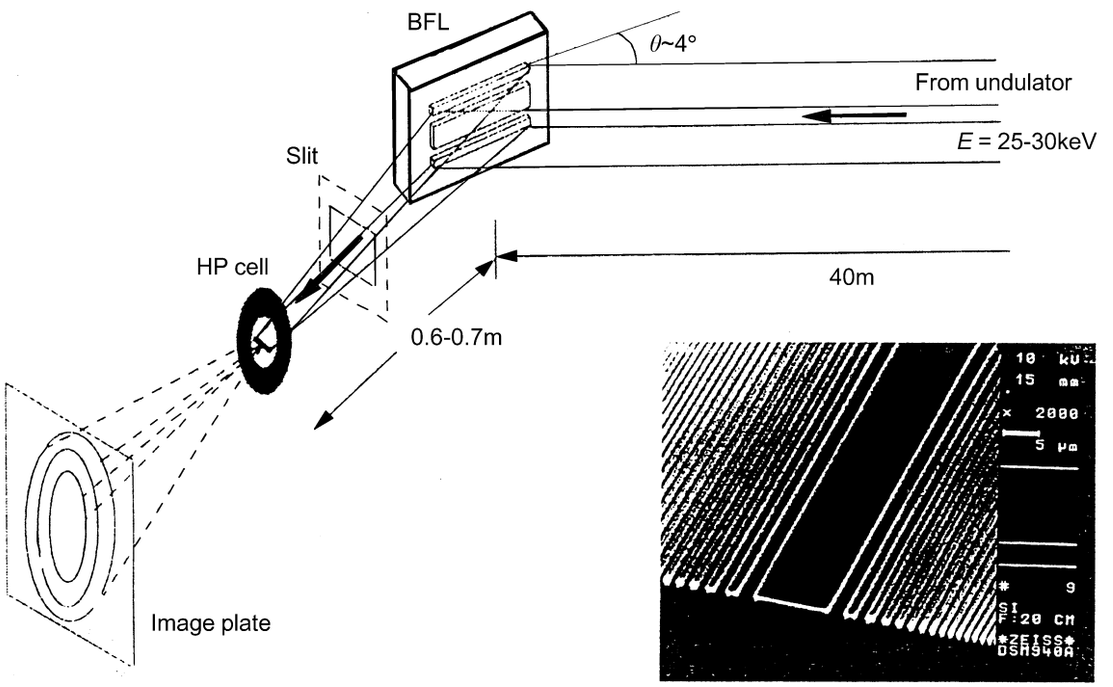

Fig. 4.2.5.7. A schematic diagram of the use of a Bragg–Fresnel lens to focus hard X-rays onto a high-pressure cell. The diameter of the sample in such a cell is typically 10 µm. The insert shows a scanning electron micrograph of the surface of the Bragg–Fresnel lens.

The rapid development in computing techniques, improvements in materials of construction and experimental equipment, and the use of synchrotron-radiation sources for X-ray scattering experiments have led to the production of a number of reviews of both the theoretical and the experimental aspects of the anomalous scattering of X-rays. Review articles by Gavrila (1981), Kissel, Pratt, Kane & Roy (1985), and Creagh (1985) discuss both the theoretical and the experimental techniques for the determination of the X-ray dispersion corrections. Creagh (1986) has discussed the use of X-ray anomalous scattering for the characterization of materials, and a review by Helliwell (1984) has described the anomalous scattering by atoms contained in proteins and its use for the solution of the structure of proteins. In a number of papers, Karle (1980, 1984*a*,*b*,*c*, 1985) has recently shown how powerful dispersion techniques can be in the solution of crystal structures. Indeed, the high intensity afforded by synchrotron-radiation sources, together with improvements in specimen-handling techniques, has led to the general use of dispersion techniques for the solution of the phase problem in crystal structures. In particular, the MAD (multiple-wavelength anomalous-dispersion) technique is used extensively for the solution of such macromolecular crystal structures as proteins and the like. The origin of the technique lies in the Bijvoet relations, but the implementation and the development of the technique is due to Hendrickson (1994).

In this section, a brief discussion of the physical principles underlying the theoretical tabulations of X-ray scattering will be given. This will be followed by a discussion of experimental techniques for the determination of the dispersion corrections. In the next section, theoretical and experimentally determined values for the dispersion corrections will be compared for a number of elements.

Currently, there is some discussion about the nature of the dispersion corrections: are they to be considered to exhibit tensor characteristics? It is clear that in all the theoretical calculations the atoms are considered to be isolated, and, therefore, if there is a tensor associated with the X-ray scattering, it must be associated with the reaction of the atoms with the polarization state of the incident radiation. Since the property of polarization of the X-ray beam is described by a first-rank tensor, it follows that the form factor must be described by a second-rank tensor (Templeton, 1994). Either the detection system of the experimental equipment must be capable of resolving the change in the polarization states of the incident and scattered radiation, or the incident radiation must be plane polarized for this property to be observable. Except for certain diffractometers at synchrotron-radiation sources, or for specially designed conventional laboratory equipment, it is not possible to determine the polarization states before and after scattering.

To a very good approximation, therefore, one can describe the form factor as being made up of a number of separate components, the largest of which is a zeroth-rank tensor that corresponds to the conventionally accepted description of the form factor. The magnitudes of any of the higher-order tensor components are small compared with this term. Whether or not they are observable depends on the characteristics of the diffraction system used in the experiment. The form-factor formalism in its zeroth-order mode has been used extremely successfully for the solution of crystal structures, the description of wavefields in crystals, the determination of the distribution of electron density in crystal structures, *etc*. as has been shown by Creagh (1993).

It must be stressed that all of the crystal structures solved so far have been solved using the conventionally accepted, zeroth-order, form-factor description of X-ray scattering. As well, all the data concerning the distribution of electron density within crystals have used this description.

Further discussion of this issue will be given in §4.2.6.3.3.4.

4.2.6.1. *Definitions*

4.2.6.1.1. *Rayleigh scattering*

When photons interact with atoms, a number of different scattering processes can occur. The dominant scattering mechanisms are: elastic scattering from the bound electrons (Rayleigh scattering); elastic scattering from the nucleus (nuclear Thomson scattering); virtual pair production in the field of the screened nucleus (Delbrück scattering); and inelastic scattering from the bound electrons (Compton scattering).

Of the elastic scattering processes, only Rayleigh scattering has a significant amplitude in the range of photon energies used by crystallographers (< 100 keV). Compton scattering will be discussed elsewhere (Section 4.2.4).

The essential feature of Rayleigh scattering is that the internal energy of the atom remains unchanged in the interaction. The momentum $\hbar\mathbf{k}_i$ and polarization $\boldsymbol{\varepsilon}_i$ of the incident photon may be modified during the process to $\hbar\mathbf{k}_f$ and $\boldsymbol{\varepsilon}_f$

$$(\hbar\mathbf{k}_i, \boldsymbol{\varepsilon}_i) + A \rightarrow A + (\hbar\mathbf{k}_f, \boldsymbol{\varepsilon}_f).$$

4.2.6.1.2. *Thomson scattering by a free electron*

From classical electromagnetic theory, it can be shown that the fraction of incident intensity scattered by a free electron is, at a position r, φ from the scattering electron,

$$I/I_0 = (r_e/r)^2 \tfrac{1}{2}(1 + \cos^2\varphi), \qquad (4.2.6.1)$$

where r_e is the classical radius of the electron ($= 2.817938 \times 10^{-15}$ m). The factor $\frac{1}{2}(1 + \cos^2\varphi)$ arises from the assumption that the electromagnetic wave is initially unpolarized. Should the wave be polarized, the factor is necessarily different from that given in equation (4.2.6.1).

Equation (4.2.6.1) is the basis on which the scattering power of ensembles of electrons is compared.

4.2.6.1.3. *Elastic scattering from electrons bound to atoms: the atomic scattering factor, the atomic form factor, and the dispersion corrections*

In considering the interaction of a photon with electrons bound in an atom, one assumes that each electron scatters independently of its fellows, and that the total scattering power of the atom is the sum of the contributions from all the electrons in the atom. Assuming that one can define an electron density $\rho(\mathbf{r})$ for an atom containing a single electron, one can show that the scattering power of that atom relative to the scattering power of a Thomson free electron is

$$f(\boldsymbol{\Delta}) = \int \rho(\mathbf{r}) \exp[i(\mathbf{k}_f - \mathbf{k}_i)\cdot\mathbf{r}]\,\mathrm{d}V, \qquad (4.2.6.2)$$

where

$$\boldsymbol{\Delta} = \mathbf{k}_f - \mathbf{k}_i \equiv \text{ change in photon momentum}$$
$$= 2|k|\sin(\theta/2),$$

θ being the total angle of scattering of the photon.

The scattering power for the atom relative to a free electron is referred to as the *atomic form factor* or the *atomic scattering factor* of the atom.

The result (4.2.6.2), which was derived using purely classical arguments, has been shown by Nelms & Oppenheimer (1955) to be identical to the result gained by quantum mechanics. If it is assumed that the atom has spherical symmetry,

$$f(\Delta) = 4\pi \int_0^\infty \rho(r) \frac{\sin \Delta r}{\Delta r} r^2 \, \mathrm{d}r. \tag{4.2.6.3}$$

For an atom containing Z electrons, the atomic form factor becomes

$$f(\Delta) = 4\pi \sum_{n=1}^{n=Z} \int_0^\infty \rho_n(r) \frac{\sin \Delta r}{\Delta r} r^2 \, \mathrm{d}r. \tag{4.2.6.4}$$

Exact solutions for the form factor are difficult to obtain, and therefore approximations have to be made to enable equation (4.2.6.4) to be evaluated. The two most commonly used approximations are the Thomas–Fermi (Thomas, 1927; Fermi, 1928) and the Hartree–Fock (Hartree, 1928; Fock, 1930) techniques.

In the Thomas–Fermi model, the atomic electrons are considered to be a degenerate gas obeying Fermi–Dirac statistics and the Pauli exclusion principle, the ground-state energy of the atom being equal to the zero-point energy of this gas. The average charge density can be written in terms of the radial potential function, $V(r)$, which may then be substituted into Poisson's equation, $\nabla^2 V(r) = \rho(r)/\varepsilon_0$, which can then be solved for $V(r)$ using the boundary conditions that $\lim_{r\to\infty} V(r) = 0$ and that $\lim_{r\to 0} rV(r) = Ze$.

The Thomas–Fermi charge distributions for different atoms are related to each other. If the form factor is known for a 'standard' atom for which the atomic number is Z_0 then, for an atom with atomic number Z,

$$f_Z(\mathbf{\Delta}) = (Z/Z_0) f_0(\mathbf{\Delta}'). \tag{4.2.6.5}$$

Here,

$$\Delta' = \Delta (Z/Z_0)^{1/3}.$$

The most accurate calculations of wavefunctions of many-electron atoms have been made using the self-consistent-field (Hartree–Fock) method. In this independent-particle model, each electron is assumed to move in the field of the nucleus and in an average field due to the other electrons. With this approach, the charge distribution can be written as

$$\rho(r) = \sum_{n=1}^{n=Z} \rho_n(r) = \sum_{n=1}^{n=Z} \Psi_n^*(r) \Psi_n(r), \tag{4.2.6.6}$$

where $\rho_n(r)$ is the charge-density distribution of the nth electron and $\Psi_n(r)$ is its wavefunction. The technique has been extended to include the effects of both exchange and correlation. Tables of relativistic Hartree–Fock values have been given by Cromer & Waber (1974). Their notation $F(x, Z)$ is related to the notation used earlier as follows:

$$f_Z(\Delta) \equiv F(x, Z),$$

where

$$x = \frac{|k|}{2\pi} \sin(\varphi/2) = \frac{\Delta}{4\pi}.$$

In the foregoing discussion, the fact that the electrons occupy definite energy levels within the atoms has been ignored: it has been assumed that the energy of the photon is very different from any of these energy levels. The theory for calculating the scattering power of an atom near a resonant energy level was supposed to be effectively the same as the well understood problem of the driven damped pendulum system. In this type of problem, the natural amplitude of the system was modified by a correction term (a real number) dependent on the proximity of the impressed frequency to the natural resonant frequency of the system and a loss term (an imaginary number) that was related to the damping factor for the resonant system. Thus the scattering power came to be written in the form

$$f = f_0 + \Delta f' + i\Delta f'', \tag{4.2.6.7}$$

where f_0 is the atomic scattering factor remote from the resonant energy levels, $\Delta f'$ is the real part of the anomalous-scattering factor, and $\Delta f''$ is the imaginary part of the anomalous-scattering factor. The nomenclature of (4.2.6.7) has been superseded, but one still encounters it occasionally in modern papers.

In what follows, a brief exposition of the various theories for the anomalous scattering of X-rays and descriptions of modern experimental techniques for their determination will be given. Comparisons will be made between the several theoretical and experimental results for a number of atomic species. From these comparisons, conclusions will be drawn as to the validity of the various theories and the relevance of certain experiments.

4.2.6.2. *Theoretical approaches for the calculation of the dispersion corrections*

All the theories that will be discussed here have the following assumptions in common: the elastic scattering is from an isolated neutral atom and that atom is spherically symmetrical. All but the most recent of the theoretical approaches neglect changes in polarization of the incident photon caused by the interaction of the photon with the atom. In the event, few experimental configurations are able to detect such changes in polarization, and the only observable for most experiments is the momentum change of the photon.

4.2.6.2.1. *The classical approach*

In the classical approach, electrons are thought of as occupying energy levels within the atom characterized by an angular frequency ω_n and a damping factor κ_n. The forced vibration of an electron gives rise to a dipolar radiation field, when the atomic scattering factor can be shown to be

$$f = \frac{\omega^2}{\omega^2 - \omega_n^2 - i\kappa_n \omega}. \tag{4.2.6.8}$$

If the probability that the electron is to be found in the nth orbit is g_n, the real part of the atomic scattering factor may be written as

$$\mathrm{Re}(f) = \sum_n g_n + \sum_n \frac{g_n \omega_n^2}{\omega^2 - \omega_n^2}. \tag{4.2.6.9}$$

The probability g_n is referred to as the oscillator strength corresponding to the virtual oscillator having natural frequency ω_n. Equation (4.2.6.9) may be written as

$$\mathrm{Re}(f) = f_0 + f', \tag{4.2.6.10}$$

where f_0 represents the sum of all the elements of the set of oscillator strengths and is unity for a single-electron atom. The second term may be written as

$$f' = \int_{\omega_{\kappa_i}}^\infty \frac{\omega'^2 (\mathrm{d}g_\kappa/\mathrm{d}\omega')}{\omega^2 - \omega'^2} \mathrm{d}\omega' \tag{4.2.6.11}$$

if the atom is assumed to have an infinite number of energy states. For an atom containing κ electrons, it is assumed that the overall value of f' is the coherent sum of the contribution of each individual electron, whence

$$f' = \sum_{\kappa} \int_{\omega_\kappa}^{\infty} \frac{\omega'^2 (\mathrm{d}g_\kappa/\mathrm{d}\omega')}{\omega^2 - \omega'^2} \mathrm{d}\omega' \qquad (4.2.6.12)$$

and the oscillator strength of the κth electron

$$g_\kappa = \int_{\omega_\kappa}^{\infty} \left[\frac{\mathrm{d}g}{\mathrm{d}\omega}\right]_\kappa \mathrm{d}\omega$$

is not unity, but the total oscillator strength for the atom must be equal to the total number of electrons in the atom.

The imaginary part of the dispersion correction f'' is associated with the damping of the incident wave by the bound electrons. It is therefore functionally related to the linear absorption coefficient, μ_l, which can be determined from experimental measurement of the decrease in intensity of the photon beam as it passes through a medium containing the atoms under investigation. It can be shown that the attenuation coefficient per atom μ_a is related to the density of the oscillator states by

$$\mu_a = \frac{2\pi^2 e^2}{\varepsilon_0 mc}\left[\frac{\mathrm{d}g}{\mathrm{d}\omega}\right], \qquad (4.2.6.13)$$

whence

$$f'' = \frac{\pi}{2}\omega\left[\frac{\mathrm{d}g_\kappa}{\mathrm{d}\omega}\right]. \qquad (4.2.6.14)$$

An expression linking the real and imaginary parts of the dispersion corrections can now be written:

$$f' = \frac{2}{\pi}\sum_{\kappa} P \int_{\omega_\kappa}^{\infty} \frac{\omega' f''(\omega', 0)}{\omega^2 - \omega'^2}\mathrm{d}\omega'. \qquad (4.2.6.15)$$

This is referred to as the Kramers–Kronig transform. Note that the term involving the restoring force has been omitted from this equation.

Equations (4.2.6.12), (4.2.6.14), and (4.2.6.15) are the fundamental equations of the classical theory of photon scattering, and it is to these equations that the predictions of other theories are compared.

4.2.6.2.2. *Non-relativistic theories*

The matrix element for Rayleigh scattering from an atom having a radially symmetric charge distribution may be written as

$$M = M_1(\boldsymbol{\varepsilon}_i \cdot \boldsymbol{\varepsilon}_f^*) + M_2(\boldsymbol{\varepsilon}_i \cdot \boldsymbol{\kappa}_f)(\boldsymbol{\varepsilon}_f^* \cdot \boldsymbol{\kappa}_i), \qquad (4.2.6.16)$$

where $\boldsymbol{\varepsilon}_i$ and $\boldsymbol{\varepsilon}_f$ represent the initial and final states of the photon. The matrix element M_1 represents scattering for polarizations $\boldsymbol{\varepsilon}_i$ and $\boldsymbol{\varepsilon}_f$ perpendicular to the plane of scattering and M_2 represents scattering for polarization states lying in the plane of scattering.

Averaged over polarization states, the differential scattering cross section takes the form

$$\frac{\mathrm{d}\sigma}{\mathrm{d}\Omega} = \frac{r_e^2}{2}(|M_1|^2 + |M_2|^2). \qquad (4.2.6.17)$$

Here σ is the photoelectric scattering cross section, which is related to the mass attenuation coefficient μ_m by

$$\sigma = (M/N_A)\mu_m \times 10^{-24}, \qquad (4.2.6.18)$$

where M is the molecular weight and N_A is Avogadro's number.

Using the vector potential of the wavefield $\mathbf{A}$, an expression for the perturbed Hamiltonian of a hydrogen-like atom coupled to the radiation field may be written as

$$\hat{\mathscr{H}} = \hat{\mathscr{H}}_0 - r_e c\mathbf{A}\cdot\mathbf{P} + \frac{r_e^2}{2}\mathbf{A}^2, \qquad (4.2.6.19)$$

where $\hat{\mathscr{H}}_0$ is the Hamiltonian for the unperturbed atom and $\mathbf{P} = i\hbar\nabla$.

After application of the second-order perturbation theory, the matrix element may be deduced to be

$$M = (\boldsymbol{\varepsilon}_i \cdot \boldsymbol{\varepsilon}_f^*) f_0(\Delta) + \frac{1}{m}\langle 1|T_1|1\rangle + \frac{1}{m}\langle 1|T_2|1\rangle. \qquad (4.2.6.20)$$

In this equation, the initial and final wavefunctions are designated as $\langle 1|$ and $|1\rangle$, respectively, and the terms T_1 and T_2 are given by

$$T_1 = \boldsymbol{\varepsilon}_f \cdot \mathbf{P}\exp(-i\mathbf{k}_f\cdot\mathbf{r})\frac{1}{E_1 - \mathscr{H}_0 + \hbar\omega + i\xi}\boldsymbol{\varepsilon}_i \cdot \mathbf{P}\exp(-i\mathbf{k}_i\cdot\mathbf{r})$$

and

$$T_2 = \boldsymbol{\varepsilon}_i \cdot \mathbf{P}\exp(-i\mathbf{k}_i\cdot\mathbf{r})\frac{1}{E_1 - \mathscr{H}_0 + \hbar\omega + i\xi}\boldsymbol{\varepsilon}_f \cdot \mathbf{P}\exp(-i\mathbf{k}_f\cdot\mathbf{r})$$

where ξ is an infinitesimal positive quantity.

The first term of equation (4.2.6.20) corresponds to the atomic scattering factor and is identical to the value given by classical theory. The terms involving T_1 and T_2 correspond to the dispersion corrections. Equation (4.2.6.20) contains no terms to account for radiation damping. More complete theories take the effect of the finite width of the radiating level into account.

It is necessary to realize that the atomic scattering factor depends on both the photon's frequency ω and the momentum vector $\boldsymbol{\Delta}$. To emphasize this dependence, equation (4.2.6.7) is rewritten as

$$f(\omega, \boldsymbol{\Delta}) = f_0(\boldsymbol{\Delta}) + f'(\omega, \boldsymbol{\Delta}) + if''(\omega, \boldsymbol{\Delta}). \qquad (4.2.6.21)$$

In the dipole approximation, it can be shown that

$$f'(\omega, 0) = \frac{2}{\pi}P\int_0^{\infty}\frac{\omega' f''(\omega', 0)}{\omega^2 - \omega'^2}\mathrm{d}\omega', \qquad (4.2.6.22)$$

which may be compared with equation (4.2.6.15) and

$$f''(\omega, 0) = \frac{\omega}{4\pi r_e c}\sigma(\omega), \qquad (4.2.6.23)$$

which may be compared with equation (4.2.6.14).

There is a direct correspondence between the predictions of the classical theory and the theory using second-order perturbation theory and non-relativistic quantum mechanics.

The extension of Hönl's (1933*a*,*b*) study of the scattering of X-rays by the K shell of atoms to other electron shells has been presented by Wagenfeld (1975).

In these calculations, the energy of the photon was assumed to be such that relativistic effects do not occur, nor do transitions within the discrete states of the atom occur. Transitions to continuum states do occur, and, using the analytical expressions for the wavefunctions of the hydrogen-like atom, analytical expressions may be developed for the photoelectric scattering cross sections. By expansion of the retardation factor $\exp(-i\mathbf{k}\cdot\mathbf{r})$ as the power series $1 - i\mathbf{k}\cdot\mathbf{r} - \frac{1}{2}(\mathbf{k}\cdot\mathbf{r})^2 + \ldots$, it is possible to determine dipolar, quadrupolar, and higher-order

terms in the analytical expression for the photoelectric scattering cross section.

The values of the cross section so obtained were used to calculate the values of $f'(\omega, \mathbf{\Delta})$ using the Kramers–Kronig transform [equation (4.2.6.22)] and $f''(\omega, \mathbf{\Delta})$ using equation (4.2.6.23). The work of Wagenfeld (1975) predicts that the values of $f'(\omega, \mathbf{\Delta})$ and $f''(\omega, \mathbf{\Delta})$ are functions of $\mathbf{\Delta}$. Whether or not this is a correct prediction will be discussed in Subsection 4.2.6.3.

Wang & Pratt (1983) have drawn attention to the importance of bound–bound transitions in the dispersion relation for the calculation of forward-scattering amplitudes. Their inclusion is especially important for elements with small atomic numbers. In a later paper, Wang (1986) has shown that, for silicon at the wavelengths of Mo $K\alpha$ and Ag $K\alpha_1$, values for $f'(\omega, 0)$ of 0.084 and 0.055, respectively, are obtained. These values should be compared with those listed in Table 4.2.6.4.

4.2.6.2.3. *Relativistic theories*

4.2.6.2.3.1. *Cromer and Liberman*: *relativistic dipole approach*

It is necessary to consider relativistic effects for atoms having all but the smallest atomic numbers. Cromer & Liberman (1970) produced a set of tables based on a relativistic approach to the scattering of photons by isolated atoms that was later reproduced in *IT* IV (1974). Subsequent experimental determinations drew attention to inaccuracies in these tables in the neighbourhood of absorption edges owing to the poor convergence of the Gaussian integration technique, which was used to evaluate the real part of the dispersion correction. In a later paper, Cromer & Liberman (1981) recalculated 34 instances for which the incident radiation lay close to the absorption edges of atoms using a modified integration procedure. Care should be exercised when using the Cromer & Liberman computer program, especially for calculations of $f'(\omega, 0)$ for high atomic weight elements at low photon energies. As Creagh (1990) and Chantler (1994) have shown, incorrect values of $f'(\omega, 0)$ can be calculated because an insufficient number of values of $f''(\omega, 0)$ are calculated prior to performing the Kramers–Kronig transform. In a new tabulation, Chantler (1995) presents the Cromer & Liberman data using a finer integrating grid. It should be noted that the relativistic correction is the same as that used in this tabulation.

These relativistic calculations are based on the scattering formula developed by Akhiezer & Berestetsky (1957) for the scattering amplitude for photons by a bound electron, *viz*:

$$S_{i\rightarrow f} = -2\pi i\delta(\varepsilon_1 + \hbar\omega_1 - \varepsilon_2 - \hbar\omega_2)\,\frac{4\pi(e\hbar c)^2}{2mc^2\hbar(\omega_1\omega_2)^{1/2}}\,f. \tag{4.2.6.24}$$

Here the angular frequencies of the incident and scattered photons are ω_1 and ω_2, respectively, and the initial and final energy states of the atom are ε_1 and ε_2, respectively. The scattering factor f is a complicated expression that includes the initial and final polarization states of the photon, the Dirac velocity operator, and the phase factors $\exp(i\mathbf{k}_1\cdot\mathbf{r})$ and $\exp(i\mathbf{k}_2\cdot\mathbf{r})$ for the incident and scattered waves, respectively. Summation is over all positive and negative intermediate states except those positive energy states occupied by other atomic electrons. The form of this expression is not easily related to the form-factor formalism that is most widely used by crystallographers, and a number of manipulations of the formula for the scattering factor are necessary to relate it more directly to the crystallographic formalism. In doing so, a number of assumptions and simplifications were made. Cromer & Liberman restricted their study to coherent, forward scatter in which changes in photon polarization did not occur. With these approximations, and using the electrical dipole approximation [$\exp(i\mathbf{k}\cdot\mathbf{r}) = 1$], they were able to show that

$$f(\omega, 0) = f(0) + f^+(\omega, 0) + \tfrac{5}{3}\frac{E_{\rm tot}}{mc^2} + if''(\omega, 0). \tag{4.2.6.25}$$

In equation (4.2.6.25), $f(0)$ is the atomic form factor for the case of forward scatter ($\mathbf{\Delta} = 0$), and the term $[+\frac{5}{3}(E_{\rm tot}/mc^2)]$ arises from the application of the dipole approximation to determine the contribution of bound electrons to the scattering process. The term $f''(\omega, 0)$ is related to the photoelectric scattering cross section expressed as a function of photon energy $\sigma(\hbar\omega)$ by

$$f''(\omega, 0) = \frac{mc}{4\pi\hbar e^2}\hbar\omega\,\sigma(\hbar\omega) \tag{4.2.6.26}$$

and

$$f^+(\omega, 0) = \left(\frac{1}{2\pi^2\hbar r_e c}\right)P\int_{mc^2}^{\infty}\frac{(\varepsilon^+ - \varepsilon_1)\sigma(\varepsilon + -\varepsilon_1)}{(\hbar\omega)^2 - (\varepsilon^+ - \varepsilon_1)^2}\,{\rm d}\varepsilon^+. \tag{4.2.6.27}$$

These equations may be compared with equations (4.2.6.23) and (4.2.6.22), respectively. But equation (4.2.6.25) differs from equation (4.2.6.21) by the term $\frac{5}{3}(E_{\rm tot}/mc^2)$, which is constant for each atomic species, and is related to the total Coulomb energy of the atom. Evidently, to keep the formalism the same, one must write

$$f'(\omega, 0) = f^+(\omega, 0) + \tfrac{5}{3}\frac{E_{\rm tot}}{mc^2}. \tag{4.2.6.28}$$

In Table 4.2.6.1, values of $E_{\rm tot}/mc^2$ are set out as a function of atomic number for elements ranging in atomic number from 3 to 98.

To develop their tables, Cromer & Liberman (1970) used the Brysk & Zerby (1968) computer code for the calculation of photoelectric cross sections, which was based on Dirac–Slater relativistic wavefunctions (Liberman, Waber & Cromer, 1965). They employed a value for the exchange potential of $0.667\rho(\mathbf{r})^{1/3}$ and experimental rather than computed values of the energy eigenvalues for the atoms.

The wide use of their tables by crystallographers inevitably meant that criticism of the accuracy of the tables was forthcoming on both theoretical and experimental grounds. Stibius-Jensen (1979) drew attention to the fact that the use of the dipole approximation too early in the argument caused an error of $-\frac{1}{2}Z(\hbar\omega/mc^2)^2$ in the tabulated values. More recently, Cromer & Liberman (1981) include this term in their calculations. Some experimental deficiencies of the tabulated values of $f'(\omega, 0)$ have been discussed by Cusatis & Hart (1977), Hart & Siddons (1981), Creagh (1980, 1984, 1985, 1986), Deutsch & Hart (1982), Dreier, Rabe, Malzfeldt & Niemann (1984), Bonse & Hartman-Lotsch (1984), and Bonse & Henning (1986).

In the latter two cases, the Kramers–Kronig transformation of photoelectric scattering results has been performed without taking into account the term that arises in the relativistic case for the total Coulomb energy of the atom. Although good agreement with the Cromer & Liberman tables is claimed, their failure to include this term is an implied criticism of the Cromer & Liberman tables. That this is unjustified can be seen by references to Fig. 4.2.6.2 taken from Bonse & Henning (1986), which shows that their interferometer results [which measure $f'(\omega, 0)$ directly] and the Kramers–Kronig results differ

from one another by $\sim E_{\rm tot}/mc^2$ in the neighbourhood of the K-absorption edge of niobium in the compound lithium niobate.

Further theoretical objections have been made by Creagh (1984) and Smith (1987), who has shown that the Stibius-Jensen correction is not valid, and that, when higher-order multipolar expansions and retardation are considered, the total self-energy correction becomes $E_{\rm tot}/mc^2$ rather than $\frac{5}{3}E_{\rm tot}/mc^2$. Fig. 4.2.6.1 shows the variation of the self-energy correction with atomic number for the modified form factor (Creagh, 1984; Smith, 1987; Cromer & Liberman, 1970).

For the imaginary part of the dispersion correction $f''(\omega, 0)$, which depends on the calculation of the photoelectric scattering cross section, better agreement is found between theoretical results and experimental data. Details of this comparison have been given elsewhere (Section 4.2.4). Suffice it to say that Creagh & Hubbell (1990), in reporting the results of the IUCr X-ray Attenuation Project, could find no rational basis for preferring the Scofield (1973) Hartree–Fock calculations to the Cromer & Liberman (1970, 1981) and Storm & Israel (1970) Dirac–Hartree–Fock–Slater calculations.

Computer programs based on the Cromer & Liberman program (Cromer & Liberman, 1983) are in use at all the major synchrotron-radiation laboratories. Many other laboratories have also acquired copies of their program. This program must be modified to remove the incorrect Stibius–Jensen correction term, and, as will be seen later, the energy term should be modified to be $E_{\rm tot}/mc^2$.

Table 4.2.6.1. *Values of E_{tot}/mc^2 listed as a function of atomic number Z*

Z	Symbol	$E_{\rm tot}/mc^2$
3	Li	−0.0004
4	Be	−0.0006
5	B	−0.0012
6	C	−0.0018
7	N	−0.0030
8	O	−0.0042
9	F	−0.0054
10	Ne	−0.0066
11	Na	−0.0084
12	Mg	−0.0110
13	Al	−0.0125
14	Si	−0.0158
15	P	−0.0180
16	S	−0.0210
17	Cl	−0.0250
18	Ar	−0.0285
19	K	−0.0320
20	Ca	−0.0362
21	Sc	−0.0410
22	Ti	−0.0460
23	V	−0.0510
24	Cr	−0.0560
25	Mn	−0.0616
26	Fe	−0.0680
27	Co	−0.0740
28	Ni	−0.0815
29	Cu	−0.0878
30	Zn	−0.0960
31	Ga	−0.104
32	Ge	−0.114
33	As	−0.120
34	Se	−0.132
35	Br	−0.141
36	Kr	−0.150
37	Rb	−0.159
38	Sr	−0.171
39	Y	−0.180
40	Zr	−0.192
41	Nb	−0.204
42	Mo	−0.216
43	Tc	−0.228
44	Ru	−0.246
45	Rh	−0.258
46	Pd	−0.270
47	Ag	−0.285
48	Cd	−0.300
49	In	−0.318
50	Sn	−0.330
51	Sb	−0.348
52	Te	−0.363
53	I	−0.384
54	Xe	−0.396
55	Cs	−0.414
56	Ba	−0.438
57	La	−0.456
58	Ce	−0.474
59	Pr	−0.492
60	Nd	−0.516
61	Pm	−0.534
62	Sm	−0.558
63	Eu	−0.582
64	Gd	−0.610
65	Tb	−0.624
66	Dy	−0.648
67	Ho	−0.672
68	Er	−0.696
69	Tm	−0.723
70	Yb	−0.750
71	Lu	−0.780
72	Hf	−0.804
73	Ta	−0.834
74	W	−0.864
75	Re	−0.900
76	Os	−0.919
77	Ir	−0.948
78	Pt	−0.984
79	Au	−1.014
80	Hg	−1.046
81	Tl	−1.080
82	Pb	−1.116
83	Bi	−1.149
84	Po	−1.189
85	At	−1.224
86	Rn	−1.260
87	Fr	−1.296
88	Ra	−1.332
89	Ac	−1.374
90	Th	−1.416
91	Pa	−1.458
92	U	−1.470
93	Np	−1.536
94	Pu	−1.584
95	Am	−1.626
96	Cm	−1.669
97	Bk	−1.716
98	Cf	−1.764

4.2.6.2.3.2. *The scattering matrix formalism*

Kissel, Pratt & Roy (1980) have developed a computer program based on the second-order S-matrix formalism suggested by Brown, Peierls & Woodward (1955). Their aim was to provide a prescription for the accurate ($\sim$1%) prediction of the total-atom Rayleigh scattering amplitudes.

Their model treats the elastic scattering as the sum of bound electron, nuclear, and Delbrück scattering cross sections, and treats the Rayleigh scattering by considering second-order, single-electron transitions from electrons bound in a relativistic, self-consistent, central potential. This potential was a Dirac–Hartree–Fock–Slater potential, and exchange was included by use of the Kohn & Sham (1965) exchange model. They omitted radiative corrections.

In principle, the observables in an elastic scattering process are momentum ($\hbar\mathbf{k}$) and polarization $\boldsymbol{\varepsilon}$. The complex polarization vectors $\boldsymbol{\varepsilon}$ satisfy the conditions

$$\boldsymbol{\varepsilon}^* \cdot \boldsymbol{\varepsilon} = 1'; \quad \boldsymbol{\varepsilon} \cdot \mathbf{k} = 0. \tag{4.2.6.29}$$

In quantum mechanics, elastic scattering is described in terms of a differential scattering amplitude, M, which is related to the elastic cross section by equation (4.2.6.16).

If polarization is not an observable, then the expression for the differential scattering cross section takes the form of equation (4.2.6.17). If polarization is taken into account, as may be the case when a polarizer is used on a beam scattered from a sample irradiated by the linearly polarized beam from a synchrotron-radiation source, the full equation, and not equation (4.2.6.17), must be used to compute the differential scattering cross section.

The principle of causality implies that the forward-scattering amplitude $M(\omega, 0)$ should be analytic in the upper half of the ω plane, and that the dispersion relation

$$\text{Re } M(\omega, 0) = \frac{2\omega^2}{\pi} \int_0^\infty \frac{\text{Im } M(\omega', 0)}{\omega'(\omega'^2 - \omega^2)} \text{d}\omega' \tag{4.2.6.30}$$

should hold, with the consequence that

$$\text{Re } M(\infty, 0) = -\frac{2}{\pi} \int_0^\infty \frac{\text{Im } M(\omega', 0)}{\omega'} \text{d}\omega'. \tag{4.2.6.31}$$

This may be rewritten as

$$M(\omega, 0) - M(\infty, 0) = f'(\omega, 0) + if''(\omega, 0), \qquad (4.2.6.32)$$

with the value of $f'(\omega, 0)$ defined by equation (4.2.6.15). Using the conservation of probability,

$$\text{Im } M(\omega, 0) = \frac{\omega}{4\pi r_e c}\sigma_{\text{tot}}, \qquad (4.2.6.33)$$

which is to be compared with equation (4.2.6.23).

Starting with Furry's extension of the formalism of quantum mechanics proposed by Feynman and Dyson, the total Rayleigh amplitude may be written as

$$M_n = \sum_p \left[\frac{\langle n|T_1^*|p\rangle\langle p|T_1|n\rangle}{E_n - E_p + \hbar\omega} + \frac{\langle n|T_2|p\rangle\langle n|T_2^*|p\rangle}{E_n - E_p + \hbar\omega} \right], \qquad (4.2.6.34)$$

where

$$T_1 = \boldsymbol{\alpha} \cdot \boldsymbol{\varepsilon}_i \cdot \exp(i\mathbf{k}_i \cdot \mathbf{r})$$

and

$$T_2 = \boldsymbol{\alpha} \cdot \boldsymbol{\varepsilon}_f^* \cdot \exp(-i\mathbf{k}_f \cdot \mathbf{r}).$$

The $|p\rangle$ are the complete set of bound and continuum states in the external field of the atomic potential. Singularities occur at all photon energies that correspond to transitions between bound $|n\rangle$ and bound state $|p\rangle$. These singularities are removed if the finite widths of these states are considered, and the energies E are replaced by $iE\Gamma/2$, where Γ is the total (radiative plus non-radiative) width of the state (Gavrila, 1981). By use of the formalism suggested by Brown *et al.* (1955), it is possible to reduce the numerical problems to one-dimensional radial integrals and differential equations. The required multipole expansions of T_1 and the specification of the radial perturbed orbitals that are characterized by angular-momentum quantum numbers have been discussed by Kissel (1977). Ultimately, all the angular dependence on the photon scattering angle is written in terms of the associated Legendre functions, and all the energy dependence is in terms of multipole amplitudes.

Solutions are not found for the inhomogeneous radial wave equations, and Kissel (1977) expressed the solution as the linear sum of two solutions of the homogeneous equation, one of which was regular at the origin and the other regular at infinity.

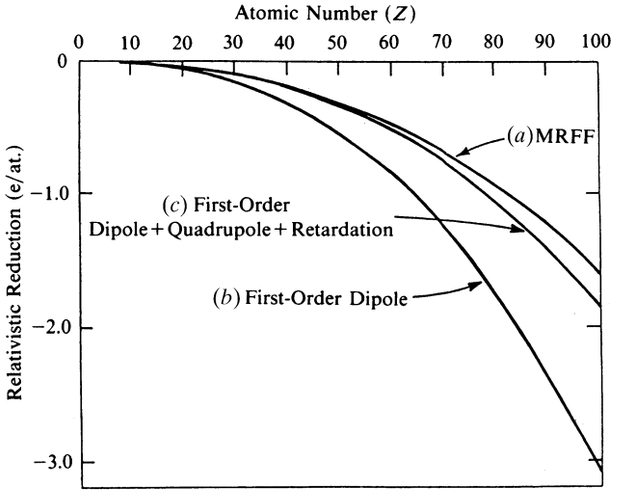

Fig. 4.2.6.1. The relativistic correction in electrons per atom for: (*a*) the modified form-factor approach; (*b*) the relativistic multipole approach; (*c*) the relativistic dipole approach.

Because excessive amounts of computer time are required to use these direct techniques for calculating the amplitudes from all the subshells, simpler methods are usually used for calculating outer-shell amplitudes. Kissel & Pratt (1985) used estimates for outer-shell amplitudes based on the predictions of the modified form-factor approach. A tabulation of the modified relativistic form factors has been given by Schaupp, Schumacher, Smend, Rullhusen & Hubbell (1983).

Because of the generality of their approach, the computer time required for the calculation of the scattering amplitudes for a particular energy is quite long, so that relatively few calculations have been made. Their approach, however, does not confine itself solely to the problem of forward scattering of photons as does the Cromer & Liberman (1970) approach. Using their model, Kissel *et al.* (1980) have been able to show that it is incorrect to assign a dependence of the dispersion corrections on the scattering vector $\boldsymbol{\Delta}$. This is at variance with some established crystallographic practices, in which the dispersion corrections are accorded the same dependence on $\boldsymbol{\Delta}$ as $f_0(\boldsymbol{\Delta})$, and also at

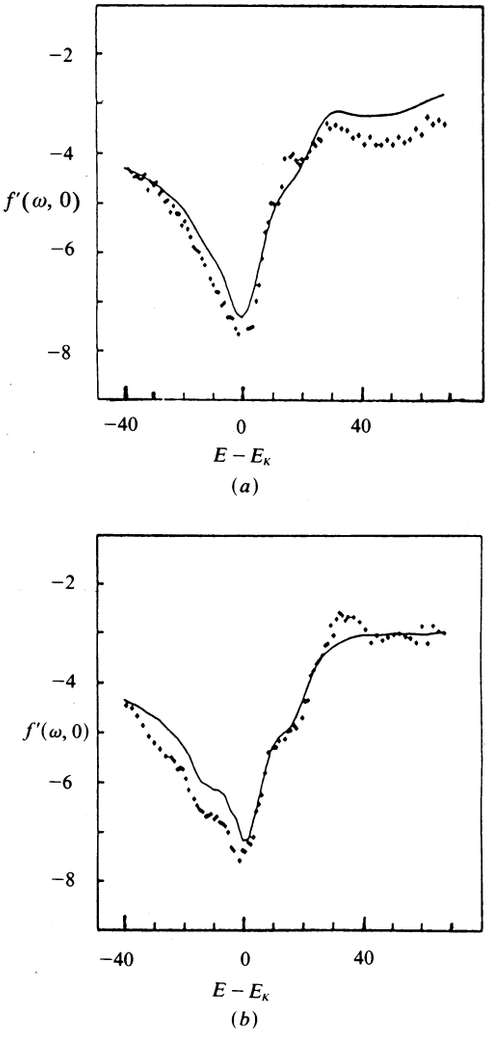

Fig. 4.2.6.2. Measured values of $f'(\omega, 0)$ at the *K*-edge of Nb in $LiNbO_3$ and the Kramers–Kronig transformation of $f''(\omega, 0)$. The curve is obtained by transformation and the points are measured by interferometry. For (*a*), the polarization of the incident radiation is parallel to the hexagonal *c* axis, and for (*b*) it is at right angles to the hexagonal *c* axis. After Bonse & Henning (1986). Note that the distortion of the dispersion curve is due to X-ray absorption near-edge structure (XANES) effects (Section 4.2.4).

variance with the predictions of Wagenfeld's (1975) non-relativistic model.

4.2.6.2.4. *Intercomparison of theories*

A discussion of the validity of the non-relativistic dipole approximation for the calculation of forward Rayleigh scattering amplitudes has been given by Roy & Pratt (1982). They compared their relativistic multipole calculations with the relativistic dipole approximation and with the non-relativistic dipole approximation for two elements, silver and lead. They concluded that a relativistic correction to the form factor of order $(Z\alpha)^2$ persists in the high-energy limit, and that this constant correction accounts for much of the deviation from the non-relativistic dipole approximation at all energies above threshold. In addition, their results illustrate that cancelling occurs amongst the relativistic, retardation, and higher multipole contributions to the scattering amplitude. This implies that care must be taken in assessing where to terminate the series that describes the multipolarity of the scattering process.

In a later paper, Roy, Kissel & Pratt (1983) discussed the elastic photon scattering for small momentum transfers and the validity of the form-factor theories. In this paper, which compares the relativistic modified form factor with experimental results for lead and a relativistic form factor and the tabulation by Hubbell, Veigele, Briggs, Brown, Cromer & Howerton (1975), it is shown that the modified relativistic form-factor approach gives better agreement with experiment for high momentum transfers ($< 104\,\text{Å}^{-1}$) than the non-relativistic, form-factor theories.

Kissel *et al*. (1980) used the *S*-matrix technique to calculate the real part of the forward-scattering amplitude $f'(\omega, 0)$ for the inert gases at the wavelength of Mo $K\alpha_1$. These values are compared with the predictions of the relativistic dipole theory (RDP) and the relativistic multipole theory (RMP) in Table 4.2.6.2(*a*). In most cases, the agreement between the *S* matrix and the RMP theory is excellent, considering the differences in the methodology of the two sets of calculations. Table 4.2.6.2(*b*) shows comparisons of the real part of the forward-scattering amplitude $f''(\omega, 0)$ calculated for the atoms aluminium, silicon, zinc, germanium, silver, samarium, tantalum and lead using the approach of Kissel *et al*. (1980) with that of Cromer & Liberman (1970, 1981), with tabulations by Wagenfeld (1975), and with values taken from the tables in this section. Although reasonably satisfactory agreement exists between the relativistic values, large differences exist between the non-relativistic value (Wagenfeld, 1975) and the relativistic values. The major difference between the relativistic values occurs because of differences in estimation of the self-consistent-field term, which is proportional to E_{tot}/mc^2. The Cromer & Liberman (1970) relativistic dipole value is $+\frac{5}{3}(E_{\text{tot}}/mc^2)$, whereas the tabulation in this section uses the relativistic multipole value of $(+E_{\text{tot}}/mc^2)$. This causes a vertical shift of the curve, but does not alter its shape. Should better estimates of the self-energy term be found, the correction is simply that of adding a constant to each value of $f'(\omega, 0)$ for each atomic species. There is a significant discrepancy between the Kissel *et al*. (1980) result for ^{62}Sm and the other theoretical values. This is the only major point of difference, however, and the results are better in accord with the relativistic multipole approach than with the relativistic dipole approach. Note that the relativistic multipole approach does not include the Stibius-Jensen correction, which alters the shape of the curve.

In §4.2.6.3.3, some examples are given to illustrate the extent to which predictions of these theories agree with experimental data for $f'(\omega, 0)$.

That there is little to choose between the different theoretical approaches where the calculation of $f''(\omega, 0)$ is concerned is illustrated in Table 4.2.6.3. In most cases, the agreement between the scattering matrix, relativistic dipole, and relativistic multipole values is within 1%. In contrast, there are some significant differences between the relativistic and the non-relativistic values of $f''(\omega, 0)$. The extent of the discrepancies is greater the higher the atomic number, as one might expect from the assumptions made in the formulation of the non-relativistic model. Some detailed comparisons of theoretical and experimental data for linear attenuation coefficients [proportional to $f''(\omega, 0)$] have been given by Creagh & Hubbell (1987) for silicon, and for copper and carbon by Gerward (1982, 1983). These tend to confirm the assertion that, at the 1% level of accuracy, there is little to choose between the various relativistic models for computing scattering cross sections.

Further discussion of this is given in §4.2.6.3.3.

4.2.6.3. *Modern experimental techniques*

The atomic scattering factor enters directly into expressions for such macroscopic material properties as the *refractive index*, n, and the *linear attenuation coefficient*, μ_l. The refractive index depends on the dielectric susceptibility χ through

$$n = (1 + \chi)^{1/2}, \tag{4.2.6.35}$$

where

$$\chi = -\frac{r_e\lambda^2}{\pi}\sum_j N_j f_j(\omega, \mathbf{\Delta}) \tag{4.2.6.36}$$

and N_j is the number density of atoms of type j.

The imaginary part of the dispersion correction $f''(\omega, \mathbf{\Delta})$ for the case where $\mathbf{\Delta} = 0$ is related to the atomic scattering cross section through equation (4.2.6.23).

Experimental techniques that measure refractive indices or X-ray attenuation coefficients to determine the dispersion corrections involve measurements for which the scattering vector, $\mathbf{\Delta}$, is zero or close to it. Data from these experiments may be compared *directly* with data sets such as Cromer & Liberman (1970, 1981).

Other techniques measure the intensities of Bragg reflections from crystalline materials or the variation of intensities within one particular Laue reflection (*Pendellösung*). For these cases, $\mathbf{\Delta} = g_{hkl}$, the reciprocal-lattice vector for the reflection or reflections measured. These techniques can be compared only indirectly with existing relativistic tabulations, since these have been developed for the $\mathbf{\Delta} = 0$ case. Data are available for elements having atomic numbers less than 20 in the non-relativistic case (Wagenfeld, 1975).

The following sections will discuss some modern techniques for the measurement of dispersion corrections, and an intercomparison will be made between experimental data and theoretical calculations for a representative selection of atoms and at two extremes of photon energies: near to and remote from an absorption edge of those atoms.

4.2.6.3.1. *Determination of the real part of the dispersion correction*: $f'(\omega, 0)$

X-ray interferometer techniques are now used extensively for the measurement of the refractive index of materials and hence

Table 4.2.6.2(*a*). *Comparison between the S-matrix calculations of Kissel (K) (1977) and the form-factor calculations of Cromer & Liberman (C & L) (1970, 1981, 1983) and Creagh & McAuley (C & M) for the noble gases and several common metals; $f'(\omega, 0)$ values are given for two frequently used photon energies*

Energy (keV)	Element	RDP (C & L)	*S* matrix (*K*)	RMP (C & M)
17.479 (Mo $K\alpha_1$)	Ne	0.021	0.024	0.026
	Ar	0.155	0.170	0.174
	Kr	−0.652	−0.478	−0.557
	Xe	−0.684	−0.416	−0.428
22.613 (Ag $K\alpha_1$)	Al	0.032	0.039	0.041
	Zn	0.260	0.323	0.324
	Ta	−0.937	−0.375	−0.383
	Pb	−1.910	−1.034	−1.162

$f'(\omega, 0)$. All the interferometers are transmission-geometry LLL devices (Bonse & Hart, 1965, 1966*a*,*b*,*c*,*d*, 1970), and initially they were used to measure the X-ray refractive indices of such materials as the alkali halides, beryllium and silicon using the characteristic radiation emitted by sealed X-ray tubes. Measurements were made for such characteristic emissions as Ag $K\alpha_1$, Mo $K\alpha_1$, Cu $K\alpha_1$ and Cr $K\alpha_1$ by a variety of authors (Creagh & Hart, 1970; Creagh, 1970; Bonse & Hellkötter, 1969; Bonse & Materlik, 1972).

The ready availability of synchrotron-radiation sources led to the adaptation of the simple LLL interferometers to use this new radiation source. Bonse & Materlik (1975) reported measurements at DESY, Hamburg, made with a temporary adaptation of a diffraction-beam line. Recent advances in X-ray interferometry have led to the establishment of a permanent interferometer station at DESY (Bonse, Hartmann-Lotsch & Lotsch, 1983*b*). This, and many of the earlier interferometers invented by Bonse, makes its phase measurements by the rotation of a phase-shifting plate in the beams emanating from the first wafer of the interferometer.

In contrast, the LLL interferometer designed by Hart (1968) uses the movement of the position of lattice planes in the third wafer of the interferometer relative to the standing-wave field formed by the recombination of two of the diffracted beams within the interferometer. Measurements made with and without the specimen in position enabled both the refractive index and the linear attenuation coefficient to be determined. The use of energy-dispersive detection meant that these parameters could be determined for harmonics of the fundamental frequency to which the interferometer was tuned (Cusatis & Hart, 1975, 1977). Subsequently, measurements have been made by Siddons & Hart (1983) and Hart & Siddons (1981) for zirconium, niobium, nickel, and molybdenum. Hart (1985) planned to provide detailed dispersion curves for a large number of elements capable of being rolled into thin foils.

Both types of interferometers have yielded data of high quality, and accuracies better than 0.2 electrons have been claimed for measurements of $f'(\omega, 0)$ in the neighbourhood of the *K*- and *L*-absorption edges of a number of elements. The energy window has been claimed to be as low as 0.3 eV in width. However, on the basis of the measured values, it would seem that the width of the energy window is more likely to be about 2 eV for a primary wavelength of 5 keV.

Table 4.2.6.2(*b*). *A comparison of the real part of the forward-scattering amplitudes computed using different theoretical approaches: KPR (Kissel et al., 1980); C & L (Cromer & Liberman, 1970, 1981); W (Wagenfeld, 1975); and C & M (this data set)*

		$f'(\omega, 0)$				
			C & L			
Atom	Radiation	KPR	1970	1981	*W*	C & M
^{13}Al	Cr $K\alpha_1$	13.320	13.328	13.316	13.376	13.326
	Cu $K\alpha_1$	13.209	13.204	13.203	13.235	13.213
	Ag $K\alpha_1$	13.039	13.032	13.020	13.078	13.041
^{14}Si	Cr $K\alpha_1$		14.333	14.354	14.441	14.365
	Cu $K\alpha_1$		14.244	14.242	14.282	14.254
	Ag $K\alpha_1$		14.042	14.029	14.071	14.052
^{30}Zn	Cr $K\alpha_1$	29.161	29.316	29.314		29.383
	Cu $K\alpha_1$	28.369	28.388	28.383		28.451
	Ag $K\alpha_1$	30.323	30.260	30.232		30.324
^{32}Ge	Cr $K\alpha_1$		31.538	31.538	30.20	31.614
	Cu $K\alpha_1$		30.837	30.837	31.92	30.911
	Ag $K\alpha_1$		32.228	32.228	32.14	32.302
^{47}Ag	Cu $K\alpha_1$	47.075	46.940	46.936		47.131
^{62}Sm	Ag $K\alpha_1$	58.307	56.304	56.299		56.676
^{73}Ta	Ag $K\alpha_1$	72.625	72.063	71.994		72.617
^{82}Pb	Ag $K\alpha_1$	80.966	80.090	80.012		80.832

Apparently, the ångström-ruler design is the better of the two interferometer types, since the interferometer to be mounted at the EU storage ring is to be of this type (Buras & Tazzari, 1985).

Interferometers of this type have the advantage of enabling direct measurements of both refractive index and linear attenuation coefficients to be made. The determination of the energy scale and the assessment of the energy bandpass of such a system are two factors that may influence the accuracy of this type of interferometer.

One of the oldest techniques for determining refractive indices derives from measurement of the deviation produced when a prism of the material under investigation is placed in the photon beam. Recently, a number of groups have used this technique to determine the X-ray refractive index, and hence $f'(\omega, 0)$.

Deutsch & Hart (1984*a*,*b*) have designed a novel double-crystal transmission spectrometer for which they were able to detect to high accuracy the angular rotation of one element with respect to the other by reference to the *Pendellösung* maxima that are observed in the wave field of the primary wafer. In this second paper, data gained for beryllium and lithium fluoride wedges are discussed.

Several Japanese groups have used more conventional monochromator systems having Bragg-reflecting optics to determine the refractive indices of a number of materials. Hosoya, Kawamure, Hunter & Hakano (1978; cited by Bonse & Hartmann-Lotsch, 1984) made determinations of $f'(\omega, 0)$ in the region of the *K*-absorption edge for copper. More recently, Ishida & Katoh (1982) have described the use of a multiple-reflection diffractometer for the determination of X-ray refrac-

Table 4.2.6.3. *A comparison of the imaginary part of the forward-scattering amplitudes $f''(\omega, 0)$ computed using different theoretical approaches: KPR (Kissel et al., 1980); C & L (Cromer & Liberman, 1981); W (Wagenfeld, 1975); and C & M (this data set)*

Atom	Radiation	$f'(\omega, 0)$			
		KPR	C & L	*W*	C & M
^{13}Al	Cr $K\alpha_1$	0.514	0.522		0.512
	Cu $K\alpha_1$	0.243	0.246		0.246
	Ag $K\alpha_1$	0.031	0.031		0.031
^{14}Si	Cr $K\alpha_1$		0.694	0.70	0.692
	Cu $K\alpha_1$		0.330	0.33	0.330
	Ag $K\alpha_1$		0.043	0.047	0.043
^{30}Zn	Cr $K\alpha_1$	1.370	1.373		1.371
	Cu $K\alpha_1$	0.678	0.678		0.678
	Ag $K\alpha_1$	0.932	0.938		0.938
^{32}Ge	Cr $K\alpha_1$		1.786	1.84	1.784
	Cu $K\alpha_1$		0.886	0.87	0.886
	Ag $K\alpha_1$		1.190	1.23	1.190
^{47}Ag	Cu $K\alpha_1$	4.242	4.282		4.282
^{62}Sm	Cu $K\alpha_1$	12.16	12.218		12.218
^{73}Ta	Ag $K\alpha_1$	4.403	4.399		4.399
^{82}Pb	Ag $K\alpha_1$	6.937	6.929		6.929

tive indices. Later, Katoh *et al*. (1985*a*,*b*) described its use for the measurement of $f'(\omega, 0)$ for lithium fluoride and potassium chloride at a wavelength near that of Mo $K\alpha_1$ and for germanium in the neighbourhood of its *K*-absorption edge.

Measurements of the linear attenuation coefficient μ_l over an extended energy range can be used as a basis for the determination of the real part of the dispersion correction $f'(\omega, 0)$ because of the Kramers–Kronig relation, which links $f'(\omega, 0)$ and $f''(\omega, 0)$. However, as Creagh (1980) has pointed out, even if the integration can be performed accurately [implying the knowledge of $f''(\omega, 0)$ over several decades of photon energies and the exact energy at which the absorption edge occurs], there will still be some ambiguity in the result because there still has to be the inclusion of the appropriate relativistic correction term.

The experimental procedures that must be adopted to ensure that the linear attenuation coefficients are measured correctly have been given in Subsection 4.2.3.2. One other problem that must be addressed is the accuracy to which the photon energy can be measured. Accuracy in the energy scale becomes paramount in the neighbourhood of an absorption edge where large variations in $f'(\omega, 0)$ occur for very small changes in photon energy $\hbar\omega$.

Despite these difficulties, Creagh (1977, 1978, 1982) has used the technique to determine $f'(\omega, 0)$ and $f''(\omega, 0)$ for several alkali halides and Gerward, Thuesen, Stibius-Jensen & Alstrup (1979) used the technique to measure these dispersion corrections for germanium. More recently, the technique has been used by Dreier *et al*. (1984) to determine $f'(\omega, 0)$ and $f''(\omega, 0)$ for a number of transition metals and rare-earth atoms. The experimental configuration used by them was a conventional XAFS system. Similar techniques have been used by Fuoss & Bienenstock (1981) to study a variety of amorphous materials in the region of an absorption edge.

Henke *et al*. (1982) used the Kramers–Kronig relation to compute the real part of the dispersion correction for most of the atoms in the Periodic Table, given their measured scattering cross sections. This data set was computed specifically for the soft X-ray region ($\hbar\omega < 1.5$ keV).

Linear attenuation coefficient measurements yield $f'(\omega, 0)$ directly and $f''(\omega, 0)$ indirectly through use of the Kramers–Kronig integral. Data from these experiments do not have the reliability of those from refractive-index measurements because of the uncertainty in knowing the correct value for the relativistic correction term.

None of the previous techniques is useful for small photon energies. These photons would experience considerable attenuation in traversing both the specimen and the experimental apparatus. For small photon energies or large atomic numbers, reflection techniques are used, the most commonly used technique being that of total external reflection. As Henke *et al*. (1982) have shown, when reflection occurs at a smooth (vacuum–material) interface, the refractive index of the reflecting material can be written as a single complex constant, and measurement of the angle of total external reflection may be related directly to the refractive index and therefore to $f'(\omega, \mathbf{\Delta})$. Because the X-ray refractive indices of materials are only slightly less than unity, the scattering wavevector $\mathbf{\Delta}$ is small, and the scattering angle is only a few degrees in magnitude. Assuming that there is not a strong dependence of $f'(\omega, \mathbf{\Delta})$ with $\mathbf{\Delta}$, one may consider that this technique provides an estimate of $f'(\omega, 0)$ for a photon energy range that cannot be surveyed using more precise techniques. A recent review of the use of reflectometers to determine $f'(\omega, 0)$ has been given by Lengeler (1994).

4.2.6.3.2. *Determination of the real part of the dispersion correction*: $f'(\omega, \mathbf{\Delta})$

This classification includes those experiments in which measurements of the geometrical structure factors F_{hkl} for various Bragg reflections are undertaken. Into this category fall those techniques for which the period of standing-wave fields (*Pendellösung*) and reflectivity of perfect crystals in Laue or Bragg reflection are measured. Also included are those techniques from which the atomic scattering factors are inferred from measurements of Bijvoet- or Friedel-pair intensity ratios for noncentrosymmetric crystal structures.

4.2.6.3.2.1. *Measurements using the dynamical theory of X-ray diffraction*

The development of the dynamical theory of X-ray diffraction (see, for example, Section 5 in *IT* B, 1995) and recent advances in techniques for crystal growth have enabled experimentalists to determine the geometrical structure factor F_{hkl} for a variety of materials by measuring the spacing between minima in the internal standing wave fields within the crystal (*Pendellösung*).

Two classes of *Pendellösung* experiment exist: those for which the ratio $(\lambda/\cos\theta)$ is kept constant and the thickness of the samples varies; and those for which the specimen thickness remains constant and $(\lambda/\cos\theta)$ is allowed to vary.

Of the many experiments performed using the former technique, measurements by Aldred & Hart (1973*a*,*b*) for

silicon are thought to be the most accurate determinations of the atomic form factor $f(\omega, \mathbf{\Delta})$ for that material. From these data, Price, Maslen & Mair (1978) were able to refine values of $f'(\omega, \mathbf{\Delta})$ for a number of photon energies. Recently, Deutsch & Hart (1985) were able to extend the determination of the form factor to higher values of momentum transfer ($\hbar\mathbf{\Delta}$). This technique requires for its success the availability of large, strain-free crystals, which limits the range of materials that can be investigated.

A number of experimentalists have attempted to measure *Pendellösung* fringes for parallel-sided specimens illuminated by white radiation, usually from synchrotron-radiation sources. [See, for example, Hashimoto, Kozaki & Ohkawa (1965) and Aristov, Shmytko & Shulakov (1977).] A technique in which the *Pendellösung* fringes are detected using a solid-state detector has been reported by Takama, Kobayashi & Sato (1982). Using this technique, Takama and his co-workers have reported measurements for silicon (Takama, Iwasaki & Sato, 1980), germanium (Takama & Sato, 1984), copper (Takama & Sato, 1982), and aluminium (Takama, Kobayashi & Sato, 1982). A feature of this technique is that it can be used with small crystals, in contrast to the first technique in this section. However, it does not have the precision of that technique.

Another technique using the dynamical theory of X-ray diffraction determines the integrated reflectivity for a Bragg-case reflection that uses the expression for integrated reflectivity given by Zachariasen (1945). Using this approach, Freund (1975) determined the value of the atomic scattering factor $f(\omega, \mathbf{g}_{222})$ for copper. Measurements of intensity are difficult to make, and this method is not capable of yielding results having the precisions of the *Pendellösung* techniques.

4.2.6.3.2.2. *Friedel- and Bijvoet-pair techniques*

The Bijvoet-pair technique (Bijvoet *et al.*, 1951) is used extensively by crystallographers to assist in the resolution of the phase problem in the solution of crystal structures. Measurements of as many as several hundred values for the diffracted intensities I_{hkl} for a crystal may be made. When these are analysed, the Cole & Stemple (1962) observation that the ratio of the intensities scattered in the Bijvoet or Friedel pair is independent of the state of the crystal is assumed to hold. This is a necessary assumption since in a large number of structure analyses radiation damage occurs during the course of an experiment.

For simple crystal structures, Hosoya (1975) has outlined a number of ways in which values of $f'(\omega, \mathbf{g}_{hkl})$ and $f''(\omega, \mathbf{g}_{hkl})$ may be extracted from the Friedel-pair ratios. Measurements of these corrections for atoms such as gallium, indium, arsenic and selenium have been made.

In more complicated crystal structures for which the positional parameters are known, attempts have been made to determine the anomalous-scattering corrections by least-squares-refinement techniques. Measurements of these corrections for a number of atoms have been made, *inter alia*, by Engel & Sturm (1975), Templeton & Templeton (1978), Philips, Templeton, Templeton & Hodgson (1978), Templeton, Templeton, Philips & Hodgson (1980), Philips & Hodgson (1985), and Chapuis, Templeton & Templeton (1985). There are a number of problems with this approach, not the least of which are the requirement to measure intensities accurately for a large period of time and the assumption that specimen perfection does not affect the intensity ratio. Also, factors such as crystal shape and primary and secondary extinction may adversely affect the ability to measure intensity ratios correctly. One problem that has to be addressed in this type of determination is the fact that $f'(\omega, 0)$ and $f''(\omega, 0)$ are related to one another, and cannot be refined separately.

4.2.6.3.3. *Comparison of theory with experiment*

In this section, discussion will be focused on (i) the scattering of photons having energies considerably greater than that of the *K*-absorption edge of the atom from which they are scattered, and (ii) scattering of photons having energies in the neighbourhood of the *K*-absorption edge of the atom from which they are scattered.

4.2.6.3.3.1. *Measurements in the high-energy limit* $(\omega/\omega_\kappa \rightarrow 0)$

In this case, there is some possibility of testing the validity of the relativistic dipole and relativistic multipole theories since, in the high-energy limit, the value of $f'(\omega, 0)$ must approach a value related to the total self energy of the atom ($E_{\rm tot}/mc^2$). That there is an atomic number dependent systematic error in the relativistic dipole approach has been demonstrated by Creagh (1984). The question of whether the relativistic multipole approach yields a result in better accord with the experimental data is answered in Table 4.2.6.4, where a comparison of values of $f'(\omega, 0)$ is made for three theoretical data sets (this work; Cromer & Liberman, 1981; Wagenfeld, 1975) with a number of experimental results. These include the 'direct' measurements using X-ray interferometers (Cusatis & Hart, 1975; Creagh, 1984), the Kramers–Kronig integration of X-ray attenuation data (Gerward *et al.*, 1979), and the angle-of-the-prism data of Deutsch & Hart (1984*b*). Also included in the table are 'indirect' measurements: those of Price *et al.* (1978), based on *Pendellösung* measurements, and those of Grimvall & Persson (1969). These latter data estimate $f'(\omega, \mathbf{g}_{hkl})$ and not $f'(\omega, 0)$. Table 4.2.6.4 details values of the real part of the dispersion correction for LiF, Si, Al and Ge for the characteristic wavelengths Ag $K\alpha_1$, Mo $K\alpha_1$ and Cu $K\alpha_1$. Of the atomic species listed, the first three are approaching the high-energy limit at Ag $K\alpha_1$, whilst for germanium the *K*-shell absorption edge lies between Mo $K\alpha_1$ and Ag $K\alpha_1$.

The high-energy-limit case is considered first: both the relativistic dipole and relativistic multipole theories underestimate $f'(\omega, 0)$ for LiF whereas the non-relativistic theory overestimates $f'(\omega, 0)$ when compared with the experimental data. For silicon, however, the relativistic multipole yields values in good agreement with experiment. Further, the values derived from the work of Takama *et al.* (1982), who used a *Pendellösung* technique to measure the atomic form factor of aluminium are in reasonable agreement with the relativistic multipole approach. Also, some relatively imprecise measurements by Creagh (1985) are in better accordance with the relativistic multipole values than with the relativistic dipole values.

Further from the high-energy limit (smaller values of ω/ω_κ), the relativistic multipole approach appears to give better agreement with theory. It must be reported here that measurements by Katoh *et al.* (1985*a*) for lithium fluoride at a wavelength of 0.77366 Å yielded a value of 0.018 in good agreement with the relativistic multipole value 0.017.

At still smaller values of (ω/ω_κ), the non-relativistic theory yields values considerably at variance with the experimental data, except for the case of LiF using Cu $K\alpha_1$ radiation. The relativistic multipole approach seems, in general, to be a little better than the relativistic approach, although agreement between experiment and theory is not at all good for germanium. Neither

of the experiments cited here, however, has claims to high accuracy.

In Table 4.2.6.5, a comparison is made of measurements of $f''(\omega, 0)$ derived from the results of the IUCr X-ray Attenuation Project (Creagh & Hubbell, 1987, 1990) with a number of theoretical predictions. The measurements were made on carbon, silicon and copper specimens at the characteristic wavelengths Cu $K\alpha_1$, Mo $K\alpha_1$ and Ag $K\alpha_1$. The principal conclusion that can be drawn from perusal of Table 4.2.6.5 is that only minor, non-systematic differences exist between the predictions of the several relativistic approaches and the experimental results. In contrast, the non-relativistic theory fails for higher values of atomic number.

4.2.6.3.3.2. *Measurements in the vicinity of an absorption edge*

The advent of the synchrotron-radiation source as a routine experimental tool and the deep interest that many crystallographers have in both XAFS and the anomalous-scattering determinations of crystal structures have stimulated considerable interest in the determination of the dispersion corrections in the neighbourhood of absorption edges. In this region, the interaction of the ejected photoelectron with electrons belonging to neighbouring atoms causes the modulations that are referred to as XAFS. Both $f''(\omega, 0)$ (which is directly proportional to the X-ray scattering cross section) and $f'(\omega, 0)$ [which is linked to $f''(\omega, 0)$ through the Kramers–Kronig integral] exhibit these modulations. It is at this point that one must realize that the theoretical tabulations are for the interactions of photons with *isolated* atoms. At best, a comparison of theory and experiment can show that they follow the same trend.

Measurements have been made in the neighbourhood of the absorption edges of a variety of atoms using the 'direct' techniques interferometry, Kramers–Kronig, refraction of a prism and critical-angle techniques, and by the 'indirect' refinement techniques. In Table 4.2.6.6, a comparison is made of experimental values taken at or near the absorption edges of copper, nickel and niobium with theoretical predictions. These have not been adjusted for any energy window that might be thought to exist in any particular experimental configuration. The theoretical values for niobium have been calculated at the energy at which the experimentalists claimed the experiment was conducted.

Despite the considerable experimental difficulties and the wide variety of experimental apparatus, there appears to be close agreement between the experimental data for each type of atom. There appears to be, however, for both copper and nickel, a large discrepancy between the theoretical values and the experimental values. It must be remembered that the experimental values are averages of the value of $f'(\omega, 0)$, the average being taken over the range of photon energies that pass through the device when it is set to a particular energy value. Furthermore, the exact position of the wavelength chosen may be in doubt in absolute terms, especially when synchrotron-radiation sources are used. Therefore, to be able to make a more realistic comparison between theory and experiment, the theoretical data gained using the relativistic multipole approach (this work) were averaged over a rectangular energy window of 5 eV width in the region containing the absorption edge. The rectangular shape arises because of the shape of the reflectivity curve and 5 eV was chosen as a result of (i) analysis of the characteristics of the interferometers used by Bonse *et al*. and Hart *et al*., and (ii) a statement concerning the experimental bandpass of the interferometer used by Bonse & Henning (1986). It must also be borne in mind that mechanical vibrations and thermal fluctuations can broaden the energy window and that 5 eV is not an overestimate of the width of this window. Note that for elements with atomic numbers less than 40 the experimental width is greater than the line width.

For the Bonse & Henning (1986) data, two values are listed for each experiment. Their experiment demonstrates the effect the state of polarization of the incoming photon has on the value of $f'(\omega, 0)$. Similar X-ray dichroism has been shown for sodium bromate by Templeton & Templeton (1985) and Chapuis *et al*. (1985). The theoretical values are for averaged polarization in

Table 4.2.6.4. *Comparison of measurements of the real part of the dispersion correction for LiF, Si, Al and Ge for characteristic wavelengths Ag $K\alpha_1$, Mo $K\alpha_1$ and Cu $K\alpha_1$ with theoretical predictions; the experimental accuracy claimed for the experiments is shown thus: (10) = 10% error*

Sample	Reference	$f'(\omega, 0)$		
		Cu $K\alpha_1$	Mo $K\alpha_1$	Ag $K\alpha_1$
LiF	Theory			
	This work	0.075	0.017	0.010
	Cromer & Liberman (1981)	0.068	0.014	0.006
	Wagenfield (1975)	0.080	0.023	0.015
	Experiment			
	Creagh (1984)	0.085 (5)	0.020 (10)	0.014 (10)
	Deutsch & Hart (1984*b*)	–	0.0217 (1)	0.0133 (1)
Si	Theory			
	This work	0.254	0.817	0.052
	Cromer & Liberman (1981)	0.242	0.071	0.042
	Wagenfeld (1975)	0.282	0.101	0.071
	Experiment			
	Cusatis & Hart (1975)	–	0.0863 (2)	0.0568 (2)
	Price *et al*. (1978)	–	0.085 (7)	0.047 (7)
	Gerward *et al*. (1979)	0.244 (7)	0.099 (7)	0.070 (7)
	Creagh (1984)	0.236 (5)	0.091 (5)	0.060 (5)
	Deutsch & Hart (1984*b*)	–	0.0847 (1)	0.0537 (1)
Al	Theory			
	This work	0.213	0.0645	0.041
	Cromer & Liberman (1981)	0.203	0.0486	0.020
	Wagenfeld (1975)	0.235	0.076	0.553
	Experiment			
	Creagh (1985)	–	0.065 (20)	0.044 (20)
	Takama *et al*. (1982)	0.20 (5)	0.07 (5)	0.035 (10)
Ge	Theory			
	This work	−1.089	0.155	0.302
	Cromer & Liberman (1981)	−1.167	0.062	0.197
	Wagenfeld (1975)	−1.80	−0.08	0.14
	Experiment			
	Gerward *et al*. (1979)	−1.04	0.30	0.43
	Grimvall & Persson (1969)	−1.79	0.08	0.27

Table 4.2.6.5. *Comparison of measurements of $f'(\omega, 0)$ for C, Si and Cu for characteristic wavelengths Ag $K\alpha_1$, Mo $K\alpha_1$ and Cu $K\alpha_1$ with theoretical predictions; the measurements are from the IUCr X-ray Attenuation Project Report (Creagh & Hubbell, 1987, 1990), corrected for the effects of Compton, Laue–Bragg, and small-angle scattering*

Sample	Reference	$f'(\omega, 0)$		
		Cu $K\alpha_1$	Mo $K\alpha_1$	Ag $K\alpha_1$
^{6}C	Theory			
	This work	0.0091	0.0016	0.0009
	Cromer & Liberman (1981)	0.0091	0.0016	0.0009
	Wagenfeld (1975)	–	–	–
	Scofield (1973)	0.0093	0.0016	0.0009
	Storm & Israel (1970)	0.0090	0.0016	0.0009
	Experiment			
	IUCr Project	0.0093	0.0016	0.0009
^{14}Si	Theory			
	This work	0.330	0.070	0.043
	Cromer & Liberman (1981)	0.330	0.0704	0.0431
	Wagenfeld (1975)	0.330	0.071	0.044
	Scofield (1973)	0.332	0.0702	0.0431
	Storm & Israel (1970)	0.331	0.0698	0.0429
	Experiment			
	IUCr Project	0.332	0.0696	0.0429
^{29}Cu	Theory			
	This work	0.588	1.265	0.826
	Cromer & Liberman (1981)	0.589	1.265	0.826
	Scofield (1973)	0.586	1.256	0.826
	Experiment			
	IUCr Project	0.588	1.267	0.826

the incident photon beam. Another important feature is the difference of 0.16 electrons between the Kramers–Kronig and the interferometer values. Bonse & Henning (1986) did not add the relativistic correction term to their Kramers–Kronig values. Inclusion of this term would have reduced the quoted values by 0.20, bringing the two data sets into close agreement with one another.

Katoh *et al*. (1985*b*) have made measurements spanning the *K*-absorption edge of germanium using the deviation by a prism method, and these data have been shown to be in excellent agreement with the theory on which these tables are based (Creagh, 1993). In contrast, the theoretical approach of Pratt, Kissell & Bergstrom (1994) does not agree so well, especially near to, and at higher photon energies, than the *K*-edge energy. Also, Chapuis *et al*. (1985) have measured the dispersion corrections for holmium in $[HoNa(edta)]\cdot 8H_2O$ for the characteristic emission lines Cu $K\alpha_1$, Cu $K\alpha_2$, Cu $K\beta$, and Mo $K\alpha_1$ using a refinement technique. Their results are in reasonable agreement with the relativistic multipole theory, *e.g.* for $f'(\omega, \mathbf{\Delta})$ at the wavelength of Cu $K\alpha_1$ experiment gives $-(16.0 \pm 0.2)$ whereas the relative multipole approach yields -15.0. For Cu $K\alpha_2$, experiment yields $-(13.9 \pm 0.3)$ and theory gives -13.67. The discrepancy between theory and experiment may well be explained by the oxidation state of the holmium ion, which is in the form Ho^{3+}. The oxidation state of an atom affects both the position of the absorption edge and the magnitude of the relativistic correction. Both of these will have a large influence on the value of $f'(\omega, \mathbf{\Delta})$ in the neighbourhood of the absorption edge, Another problem that may be of some significance is the natural width of the absorption edge, about 60 eV. What is remarkable is the extent of the agreement between theory and experiment given the nature of the experiment. In these experiments, the intensities of many reflections (usually nearly 1000) are analysed and compared. Such a procedure can be followed only if there is no dependence of $f'(\omega, \mathbf{\Delta})$ on $\mathbf{\Delta}$.

It had often been thought that the dispersion corrections should exhibit some functional dependence on scattering angle. Indeed, some texts ascribe to these corrections the same functional dependence on angle of scattering as the form factor. A fundamental dependence was also predicted theoretically on the basis of non-relativistic quantum mechanics (Wagenfeld, 1975). This prediction is not supported by modern approaches using relativistic quantum mechanics [see, for example, Kissel *et al*. (1980)]. Reference to Tables 4.2.6.4 and 4.2.6.6 shows that the agreement between experimental values derived from diffraction experiments and those derived from 'direct' experiments is excellent. They are also in excellent agreement with the recent calculations, using relativistic quantum mechanics, so that it may be inferred that there is indeed no functional dependence of the dispersion corrections on scattering angle. Moreover, Suortti, Hastings & Cox (1985) have recently demonstrated that $f'(\omega, \mathbf{\Delta})$ was independent of $\mathbf{\Delta}$ in a powder-diffraction experiment using a nickel specimen.

4.2.6.3.3.3. *Accuracy in the tables of dispersion corrections*

Experimentalists must be aware of two potential sources of error in the values of $f'(\omega, 0)$ listed in Table 4.2.6.5. One is computational, arising from the error in calculating the relativistic correction. Stibius-Jensen (1980) has suggested that this error may be as large as $\pm 0.25(E_{\rm tot}/mc^2)$. This means, for example, that the real part of the dispersion correction $f'(\omega, 0)$ for lead at the wavelength of 0.55936 Å is $-(1.168 \pm 0.146)$. The effect of this error is to shift the dispersion curve vertically without distorting its shape. Note, however, that the direction of the shift is either up or down for all atoms: the effect of multipole cancellation and retardation will be in the same direction for all atoms.

The second possible source of error occurs because the position of the absorption edge varies somewhat depending on the oxidation state of the scattering atom. This has the effect of displacing the dispersion curve laterally. Large discrepancies may occur for those regions in which the dispersion corrections are varying rapidly with photon energy, *i.e.* near absorption edges.

It must also be borne in mind that in the neighbourhood of an absorption edge polarization effects may occur. The tables are valid only for average polarization.

4.2.6.3.3.4. *Towards a tensor formalism*

The question of how best to describe the interaction of X-rays with crystalline materials is quite difficult to answer. In the form factor formalism, the atoms are supposed to scatter as though they are isolated atoms situated at fixed positions in the unit cell. In the vast majority of cases, the polarization on scattering is not detected, and only the scattered intensities are measured. From the scattered intensities, the distribution of the electron density within the unit cell is calculated, and the difference between the form-factor model and that calculated from the intensities is taken as a measure of the nature and location of chemical bonds between atoms in the unit cell.

Table 4.2.6.6. *Comparison of $f'(\omega_A, 0)$ for copper, nickel, zirconium, and niobium for theoretical and experimental data sets; in this table: BR ≡ Bragg reflection; IN ≡ interferometer; KK ≡ Kramers–Kronig; CA = critical angle; and REF = reflectivity; measurements have been made for the K-absorption edges of copper and nickel and near the K-absorption edges of zirconium and niobium; claimed experimental errors are not worse than 5%*

Reference	Method	$f'(\omega_A, 0)$			
		Cu	Ni	Nb	Zr
Experiment					
Freund (1975)	BR	−8.2			
Begum, Hart, Lea & Siddons (1986)	IN	−7.84	−7.66		
Bonse & Materlik (1972)	IN		−8.1		
Bonse, Hartmann-Lotsch & Lotsch (1983*a*)	IN	−8.3			
Hart & Siddons (1981)	IN	−9.3	−9.2	−4.396	−6.670
Kawamura & Fukimachi (1978; cited in Bonse & Hartmann-Lotsch, 1984)	KK		−7.9		
Dreier *et al*. (1984)	KK	−8.2	−7.8		−7.83
	IN	−8.3	−8.1		
Bonse & Hartmann-Lotsch (1984)	KK	−8.3	−7.7		
Fukamachi *et al*. (1978; cited in Bonse & Hartmann-Lotsch, 1984)	KK	−8.8			
	CA	−10.0			
Bonse & Henning (1986)	IN			−7.37; −7.73	
	KK			−7.21; −7.62	
Stanglmeier, Lengeler, Weber, Gobel & Schuster (1992)	REF	−8.5	−8.1		
Creagh (1990, 1993)	REF	−8.2	−7.7		−6.8
Theory					
Cromer & Liberman (1981)		−13.50	−9.45	−4.20; −7.39	−6.207
This work		−9.5	−9.40	−4.04; −7.23	−6.056
Averaged values (5 eV) window)		−9.0	−7.53	−8.18	−6.04

This is the zeroth-order approximation to a solution, but it is in fact the only way crystal structures are solved *ab initio*.

The existence of chemical bonding imposes additional restrictions on the symmetry of lattices, and, if the associated influence this has on the complexity of energy levels is taken into account, significant changes in the scattering factors may occur in the neighbourhood of the absorption edges of the atoms comprising the crystal structure. The magnitudes of the dispersion corrections are sensitive to the chemical state, particularly oxidation state, and phenomena similar to those observed in the XAFS case (Section 4.2.4) are observed.

The XAFS interaction arising from the presence of neighbouring atoms is proportional to $f''(\omega, 0)$ and therefore is related to $f'(\omega, 0)$ through the Kramers–Kronig integral. It is not surprising that these modulations are observed in diffracted intensities in those X-ray diffraction experiments where the photon energy is scanned through the absorption edge of an atomic species in the crystal lattice. Studies of this type are referred to as diffraction absorption fine structure (DAFS) experiments. A recent review of work performed using counter techniques has been given by Sorenson (1994). Creagh & Cookson (1995) have described the use of imaging-plate techniques to study the structure and site symmetry using the DAFS technique. This technique has the ability to discriminate between different lattice sites in the unit cell occupied by an atomic species. XAFS cannot make this discrimination. The DAFS modulations are small perturbations to the diffracted intensities. They are, however, significantly larger than the tensor effects described in the following paragraphs.

In the case where the excited state lacks high symmetry and is oriented by crystal bonding, the scattering can no longer be described by a scalar scattering factor but must be described by a symmetric second-rank tensor. The consequences of this have been described by Templeton (1994). It follows therefore that material media can be optically active in the X-ray region. Hart (1994) has used his unique polarizing X-ray optical devices to study, for example, Faraday rotation in such materials as iron, in the region of the iron *K*-absorption edge, and cobalt(III) bromide monohydrate in the region of the cobalt *K*-absorption edge.

The theory of anisotropy in anomalous scattering has been treated extensively by Kirfel (1994), and Morgenroth, Kirfel

Table 4.2.6.7. *List of wavelengths, energies, and linewidths used in compiling the table of dispersion corrections (a) Agarwal (1979); (b) Deutsch & Hart (1982)*

Radiation	Wavelength (Å)	Energy (keV)	Linewidth (eV)
^{79}Au $K\alpha_1$	0.180195	68.803	46 (*a*)
^{74}W $K\alpha_1$	0.209010	59.318	43 (*a*)
^{73}Ta $K\alpha_1$	0.215947	57.412	42 (*a*)
^{47}Ag $K\alpha_1$	0.559360	22.165	7 (*a*)
^{42}Mo $K\alpha_1$	0.709260	17.480	4 (*a*)
^{29}Cu $K\alpha_1$	1.540520	8.04792	2.61 (*b*)
^{27}Co $K\alpha_1$	1.788965	6.9302	1.8
^{26}Fe $K\alpha_1$	1.93597	6.4040	1.6
^{24}Cr $K\alpha_1$	2.289620	5.4149	1.5
^{22}Ti $K\alpha_1$	2.748510	4.5108	1.4

Table 4.2.6.8. *Dispersion corrections for forward scattering*

Wavelength (Å)		2.748510	2.289620	1.935970	1.788965	1.540520	0.709260	0.559360	0.215947	0.209010	0.180195
Li	$f' =$	0.0035	0.0023	0.0015	0.0013	0.0008	−0.0003	−0.0004	−0.0006	−0.0006	−0.0006
	$f'' =$	0.0013	0.0008	0.0006	0.0005	0.0003	0.0001	0.0000	0.0000	0.0000	0.0000
Be	$f' =$	0.0117	0.0083	0.0060	0.0052	0.0038	0.0005	0.0001	−0.0005	−0.0005	−0.0005
	$f'' =$	0.0050	0.0033	0.0023	0.0019	0.0014	0.0002	0.0001	0.0000	0.0000	0.0000
B	$f' =$	0.0263	0.0190	0.0140	0.0121	0.0090	0.0013	0.0004	−0.0009	−0.0009	−0.0010
	$f'' =$	0.0139	0.0094	0.0065	0.0055	0.0039	0.0007	0.0004	0.0000	0.0000	0.0000
C	$f' =$	0.0490	0.0364	0.0273	0.0237	0.0181	0.0033	0.0015	−0.0012	−0.0013	−0.0014
	$f'' =$	0.0313	0.0213	0.0148	0.0125	0.0091	0.0016	0.0009	0.0001	0.0001	0.0001
N	$f' =$	0.0807	0.0606	0.0461	0.0403	0.0311	0.0061	0.0030	−0.0020	−0.0020	−0.0023
	$f'' =$	0.0606	0.0416	0.0293	0.0248	0.0180	0.0033	0.0019	0.0002	0.0002	0.0001
O	$f' =$	0.1213	0.0928	0.0716	0.0630	0.0492	0.0106	0.0056	−0.0025	−0.0026	−0.0030
	$f'' =$	0.1057	0.0731	0.0518	0.0440	0.0322	0.0060	0.0036	0.0004	0.0004	0.0003
F	$f' =$	0.1700	0.1324	0.1037	0.0920	0.0727	0.0171	0.0096	−0.0027	−0.0028	−0.0034
	$f'' =$	0.1710	0.1192	0.0851	0.0725	0.0534	0.0103	0.0061	0.0007	0.0007	0.0005
Ne	$f' =$	0.2257	0.1793	0.1426	0.1273	0.1019	0.0259	0.0152	−0.0025	−0.0028	−0.0037
	$f'' =$	0.2621	0.1837	0.1318	0.1126	0.0833	0.0164	0.0098	0.0012	0.0011	0.0008
Na	$f' =$	0.2801	0.2295	0.1857	0.1670	0.1353	0.0362	0.0218	−0.0028	−0.0031	−0.0044
	$f'' =$	0.3829	0.2699	0.1957	0.1667	0.1239	0.0249	0.0150	0.0019	0.0017	0.0012
Mg	$f' =$	0.3299	0.2778	0.2309	0.2094	0.1719	0.0486	0.0298	−0.0030	−0.0034	−0.0052
	$f'' =$	0.5365	0.3812	0.2765	0.2373	0.1771	0.0363	0.0220	0.0028	0.0026	0.0018
Al	$f' =$	0.3760	0.3260	0.2774	0.2551	0.2130	0.0645	0.0406	−0.0020	−0.0026	−0.0050
	$f'' =$	0.7287	0.5212	0.3807	0.3276	0.2455	0.0514	0.0313	0.0040	0.0037	0.0027
Si	$f' =$	0.3921	0.3647	0.3209	0.2979	0.2541	0.0817	0.0522	−0.0017	−0.0025	−0.0055
	$f'' =$	0.9619	0.6921	0.5081	0.4384	0.3302	0.0704	0.0431	0.0056	0.0052	0.0038
P	$f' =$	0.3821	0.3898	0.3592	0.3388	0.2955	0.1023	0.0667	−0.0002	−0.0012	−0.0050
	$f'' =$	1.2423	0.8984	0.6628	0.5731	0.4335	0.0942	0.0580	0.0077	0.0071	0.0052
S	$f' =$	0.3167	0.3899	0.3848	0.3706	0.3331	0.1246	0.0826	0.0015	0.0003	−0.0045
	$f'' =$	1.5665	1.1410	0.8457	0.7329	0.5567	0.1234	0.0763	0.0103	0.0096	0.0069
Cl	$f' =$	0.1832	0.3508	0.3920	0.3892	0.3639	0.1484	0.0998	0.0032	0.0017	−0.0042
	$f'' =$	1.9384	1.4222	1.0596	0.9202	0.7018	0.1585	0.0984	0.0134	0.0125	0.0091
Ar	$f' =$	−0.0656	0.2609	0.3696	0.3880	0.3843	0.1743	0.1191	0.0059	0.0041	−0.0030
	$f'' =$	2.3670	1.7458	1.3087	1.1388	0.8717	0.2003	0.1249	0.0174	0.0162	0.0118
K	$f' =$	−0.5083	0.0914	0.3068	0.3532	0.3868	0.2009	0.1399	0.0089	0.0067	−0.0017
	$f'' =$	2.8437	2.1089	1.5888	1.3865	1.0657	0.2494	0.1562	0.0219	0.0204	0.0149
Ca	$f' =$	−1.3666	−0.1987	0.1867	0.2782	0.3641	0.2262	0.1611	0.0122	0.0097	−0.0002
	$f'' =$	3.3694	2.5138	1.9032	0.6648	1.2855	0.3064	0.1926	0.0273	0.0255	0.0187
Sc	$f' =$	−5.4265	−0.6935	−0.0120	0.1474	0.3119	0.2519	0.1829	0.0159	0.0130	0.0015
	$f'' =$	4.0017	2.9646	2.2557	1.9774	1.5331	0.3716	0.2348	0.0338	0.0315	0.0231
Ti	$f' =$	−2.2250	−1.6394	−0.3318	−0.0617	0.2191	0.2776	0.2060	0.0212	0.0179	0.0047
	$f'' =$	0.5264	3.4538	2.6425	2.3213	1.8069	0.4457	0.2830	0.0414	0.0387	0.0284
V	$f' =$	−1.6269	−4.4818	−0.8645	−0.3871	0.0687	0.3005	0.2276	0.0259	0.0221	0.0070
	$f'' =$	0.6340	0.4575	3.0644	2.6994	2.1097	0.5294	0.3376	0.0500	0.0468	0.0344
Cr	$f' =$	−1.2999	−2.1308	−1.9210	−0.9524	−0.1635	0.3209	0.2496	0.0314	0.0272	0.0101
	$f'' =$	0.7569	0.5468	3.5251	3.1130	2.4439	0.6236	0.3992	0.0599	0.0561	0.0413
Mn	$f' =$	−1.0732	−1.5980	−3.5716	−2.0793	−0.5299	0.3368	0.2704	0.0377	0.0330	0.0139
	$f'' =$	0.8956	0.6479	0.4798	3.5546	2.8052	0.7283	0.4681	0.0712	0.0666	0.0492
Fe	$f' =$	−0.8901	−1.2935	−2.0554	−3.3307	−1.1336	0.3463	0.2886	0.0438	0.0386	0.0173
	$f'' =$	1.0521	0.7620	0.5649	0.4901	3.1974	0.8444	0.5448	0.0840	0.0787	0.0582
Co	$f' =$	−0.7307	−1.0738	−1.5743	−2.0230	−2.3653	0.3494	0.3050	0.0512	0.0454	0.0219
	$f'' =$	1.2272	0.8897	0.6602	0.5731	3.6143	0.9721	0.6296	0.0984	0.0921	0.0682
Ni	$f' =$	−0.5921	−0.9005	−1.2894	−1.5664	−3.0029	0.3393	0.3147	0.0563	0.0500	0.0244
	$f'' =$	1.4240	1.0331	0.7671	0.6662	0.5091	1.1124	0.7232	0.1146	0.1074	0.0796
Cu	$f' =$	−0.4430	−0.7338	−1.0699	−1.2789	−1.9646	0.3201	0.3240	0.0647	0.0579	0.0298
	$f'' =$	1.6427	1.1930	0.8864	0.7700	0.5888	1.2651	0.8257	0.1326	0.1242	0.0922
Zn	$f' =$	−0.3524	−0.6166	−0.9134	−1.0843	−1.5491	0.2839	0.3242	0.0722	0.0648	0.0344
	$f'' =$	1.8861	1.3712	1.0193	0.8857	0.6778	1.4301	0.9375	0.1526	0.1430	0.1063
Ga	$f' =$	−0.2524	−0.4989	−0.7701	−0.9200	−1.2846	0.2307	0.3179	0.0800	0.0721	0.0393
	$f'' =$	2.1518	1.5674	1.1663	1.0138	0.7763	1.6083	1.0589	0.1745	0.1636	0.1218
Ge	$f' =$	−0.1549	−0.3858	−0.6412	−0.7781	−1.0885	0.1547	0.3016	0.0880	0.0796	0.0445
	$f'' =$	2.4445	1.7841	1.3291	1.1557	0.8855	1.8001	1.1903	0.1987	0.1863	0.1389
As	$f' =$	−0.0687	−0.2871	−0.5260	−0.6523	−0.9300	0.0499	0.2758	0.0962	0.0873	0.0501
	$f'' =$	2.7627	2.0194	1.5069	1.3109	1.0051	2.0058	1.3314	0.2252	0.2112	0.1576
Se	$f' =$	0.0052	−0.1919	−0.4179	−0.5390	−0.7943	−0.0929	0.2367	0.1047	0.0954	0.0560
	$f'' =$	3.1131	2.2784	1.7027	1.4821	1.1372	2.2259	1.4831	0.2543	0.2386	0.1782
Br	$f' =$	0.0592	−0.1095	−0.3244	−0.4363	−0.6763	−0.2901	0.1811	0.1106	0.1026	0.0613
	$f'' =$	3.4901	2.5578	1.9140	1.6673	1.2805	2.4595	1.6452	0.2858	0.2682	0.2006
Kr	$f' =$	0.1009	−0.0316	−0.2303	−0.3390	−0.5657	−0.5574	0.1067	0.1180	0.1082	0.0668
	$f'' =$	3.9083	2.8669	2.1472	1.8713	1.4385	2.7079	1.8192	0.3197	0.3003	0.2251

Table 4.2.6.8. *Dispersion corrections for forward scattering (cont.)*

Wavelength (Å)		2.748510	2.289620	1.935970	1.788965	1.540520	0.709260	0.559360	0.215947	0.209010	0.180195
Rb	$f' =$	0.1056	0.0247	−0.1516	−0.2535	−0.4688	−0.9393	0.0068	0.1247	0.1146	0.0717
	$f'' =$	4.3505	3.1954	2.3960	2.0893	1.6079	2.9676	2.0025	0.3561	0.3346	0.2514
Sr	$f' =$	0.1220	0.1037	−0.0489	−0.1448	−0.3528	−1.5307	−0.1172	0.1321	0.1219	0.0769
	$f'' =$	4.8946	3.6029	2.7060	2.3614	1.8200	3.2498	2.2025	0.3964	0.3726	0.2805
Y	$f' =$	0.0654	0.1263	0.0138	−0.0720	−0.2670	−2.7962	−0.2879	0.1380	0.1278	0.0819
	$f'' =$	5.4198	3.9964	3.0054	2.6241	2.0244	3.5667	2.4099	0.4390	0.4128	0.3112
Zr	$f' =$	−0.0304	0.1338	0.0659	−0.0066	−0.1862	−2.9673	−0.5364	0.1431	0.1329	0.0863
	$f'' =$	5.9818	4.4226	3.3301	2.9086	2.2449	0.5597	2.6141	0.4852	0.4562	0.3443
Nb	$f' =$	−0.1659	0.1211	0.1072	0.0496	−0.1121	−2.0727	−0.8282	0.1471	0.1371	0.0905
	$f'' =$	6.5803	4.8761	3.6768	3.2133	2.4826	0.6215	2.8404	0.5342	0.5025	0.3797
Mo	$f' =$	−0.3487	0.0801	0.1301	0.0904	−0.0483	−1.6832	−1.2703	0.1487	0.1391	0.0934
	$f'' =$	7.2047	5.3484	4.0388	3.5326	2.7339	0.6857	3.0978	0.5862	0.5517	0.4177
Tc	$f' =$	−0.6073	−0.0025	0.1314	0.1164	0.0057	−1.4390	−2.0087	0.1496	0.1406	0.0960
	$f'' =$	7.8739	5.8597	4.4331	3.8799	3.0049	0.7593	3.3490	0.6424	0.6047	0.4582
Ru	$f' =$	−0.9294	−0.1091	0.1220	0.1331	0.0552	−1.2594	−5.3630	0.1491	0.1409	0.0981
	$f'' =$	8.5988	6.4069	4.8540	4.2509	3.2960	0.8363	3.6506	0.7016	0.6607	0.5014
Rh	$f' =$	−1.3551	−0.2630	0.0861	0.1305	0.0927	−1.1178	−2.5280	0.1445	0.1373	0.0970
	$f'' =$	9.3504	6.9820	5.2985	4.6432	3.6045	0.9187	0.5964	0.7639	0.7195	0.5469
Pd	$f' =$	−1.9086	−0.4640	0.0279	0.1128	0.1215	−0.9988	−1.9556	0.1387	0.1327	0.0959
	$f'' =$	10.1441	7.5938	5.7719	5.0613	3.9337	1.0072	0.6546	0.8302	0.7822	0.5955
Ag	$f' =$	−2.5003	−0.7387	−0.0700	0.0634	0.1306	−0.8971	−1.6473	0.1295	0.1251	0.0928
	$f'' =$	10.9916	8.2358	6.2709	5.5027	4.2820	1.1015	0.7167	0.9001	0.8484	0.6469
Cd	$f' =$	−3.5070	−1.1086	−0.2163	−0.0214	0.1185	−0.8075	−1.4396	0.1171	0.1147	0.0881
	$f'' =$	11.9019	8.9174	6.8017	5.9728	4.6533	1.2024	0.7832	0.9741	0.9185	0.7013
In	$f' =$	−5.1325	−1.5975	−0.4165	−0.1473	0.0822	−0.7276	−1.2843	0.1013	0.1012	0.0816
	$f'' =$	12.6310	9.6290	7.3594	6.4674	5.0449	1.3100	0.8542	1.0519	0.9922	0.7587
Sn	$f' =$	−7.5862	−2.2019	−0.6686	−0.3097	0.0259	−0.6537	−1.1587	0.0809	0.0839	0.0728
	$f'' =$	13.5168	10.3742	7.9473	6.9896	5.4591	1.4246	0.9299	1.1337	1.0697	0.8192
Sb	$f' =$	−9.2145	−3.0637	−0.9868	−0.5189	−0.0562	−0.5866	−1.0547	0.0559	0.0619	0.0613
	$f'' =$	12.7661	11.1026	8.5620	7.5367	5.8946	1.5461	1.0104	1.2196	1.1512	0.8830
Te	$f' =$	−11.6068	−4.2407	−1.4022	−0.7914	−0.1759	−0.5308	−0.9710	0.0216	0.0316	0.0435
	$f'' =$	−10.1013	11.8079	9.2067	8.1113	6.3531	1.6751	1.0960	1.3095	1.2366	0.9499
I	$f' =$	−13.9940	−5.6353	1.9032	1.1275	−0.3257	−0.4742	−0.8919	−0.0146	−0.0001	0.0259
	$f'' =$	3.4071	12.6156	9.8852	8.7159	6.8362	1.8119	1.1868	1.4037	1.3259	1.0201
Xe	$f' =$	−9.6593	−8.1899	−2.6313	−1.5532	−0.5179	−0.4205	−0.8200	−0.0565	−0.0367	0.0057
	$f'' =$	3.7063	11.7407	10.5776	9.3585	7.3500	1.9578	1.2838	1.5023	1.4195	1.0938
Cs	$f' =$	−8.1342	−10.3310	−3.5831	−2.1433	−0.7457	−0.3680	−0.7527	−0.1070	−0.0809	0.0194
	$f'' =$	4.0732	12.8551	11.2902	10.0454	7.9052	2.1192	1.3916	1.6058	1.5179	1.1714
Ba	$f' =$	−7.2079	−11.0454	−4.6472	−2.7946	−1.0456	−0.3244	−0.6940	−0.1670	−0.1335	−0.0494
	$f'' =$	4.4110	10.0919	12.0003	10.7091	8.4617	2.2819	1.5004	1.7127	1.6194	1.2517
La	$f' =$	−6.5722	−12.8190	−6.3557	−3.6566	−1.4094	−0.2871	−0.6411	−0.2363	−0.1940	−0.0835
	$f'' =$	4.7587	3.5648	12.8927	11.4336	9.0376	2.4523	1.6148	1.8238	1.7250	1.3353
Ce	$f' =$	−6.0641	−9.3304	−8.0962	−4.8792	−1.8482	−0.2486	−0.5890	−0.3159	−0.2633	−0.1222
	$f'' =$	5.1301	3.8433	11.8734	12.1350	9.6596	2.6331	1.7358	1.9398	1.8353	1.4227
Pr	$f' =$	−5.6727	−7.9841	−10.9279	−6.7923	−2.4164	−0.2180	−0.5424	−0.4096	−0.3443	−0.1666
	$f'' =$	5.5091	4.1304	9.2394	12.8653	10.2820	2.8214	1.8624	2.0599	1.9496	1.5136
Nd	$f' =$	−5.3510	−7.1451	−10.5249	−8.1618	−3.1807	−0.1943	−0.5012	−0.5194	−0.4389	−0.2183
	$f'' =$	5.9005	4.4278	9.9814	11.9121	10.9079	3.0179	1.9950	2.1843	2.0679	1.6077
Pm	$f' =$	−5.0783	−6.5334	−13.2062	−10.0720	−4.0598	−0.1753	−0.4626	−0.6447	−0.5499	−0.2776
	$f'' =$	6.3144	4.7422	3.6278	9.2324	11.5523	3.2249	2.1347	2.3143	2.1906	1.7056
Sm	$f' =$	−4.8443	−6.0570	−9.3497	−10.2609	−5.3236	−0.1638	−0.4287	−0.7989	−0.6734	−0.3455
	$f'' =$	6.7524	5.0744	3.8839	9.9412	12.2178	3.4418	2.2815	2.4510	2.3197	1.8069
Eu	$f' =$	−4.6288	−5.6630	−7.9854	−13.5405	−8.9294	−0.1578	−0.3977	−0.9903	−0.8137	−0.4235
	$f'' =$	7.2035	5.4178	4.1498	3.6550	11.1857	3.6682	2.4351	2.5896	2.4526	1.9120
Gd	$f' =$	−4.5094	−5.3778	−7.1681	−9.3863	−8.8380	−0.1653	−0.3741	−1.2279	−1.0234	−0.5140
	$f'' =$	7.6708	5.7756	4.4280	3.9016	11.9157	3.9035	2.5954	2.7304	2.5878	2.0202
Tb	$f' =$	−4.3489	−5.0951	−6.5583	−8.0413	−9.1472	−0.1723	−0.3496	−1.5334	−1.2583	−0.6165
	$f'' =$	8.1882	6.1667	4.7292	4.1674	9.1891	4.1537	2.7654	2.8797	2.7310	2.1330
Dy	$f' =$	−4.1616	−4.8149	−6.0597	−7.1503	−9.8046	−0.1892	−0.3302	−1.9594	−1.5632	−0.7322
	$f'' =$	8.6945	6.5527	5.0280	4.4320	9.8477	4.4098	2.9404	3.0274	2.8733	2.2494
Ho	$f' =$	−4.0280	−4.5887	−5.6628	−6.5338	−14.9734	−0.2175	−0.3168	−2.6705	−1.9886	−0.8709
	$f'' =$	9.2302	6.9619	5.3451	4.7129	3.7046	4.6783	3.1241	3.1799	3.0218	2.3711
Er	$f' =$	−3.9471	−4.4106	−5.3448	−6.0673	−9.4367	−0.2586	−0.3091	−5.5645	−2.6932	−1.0386
	$f'' =$	9.7921	7.3910	5.6776	5.0074	3.9380	4.9576	3.3158	0.6167	3.1695	2.4949
Tm	$f' =$	−3.9079	−4.2698	−5.0823	−5.6969	−8.0393	−0.3139	−0.3084	−2.8957	−5.6057	−1.2397
	$f'' =$	10.3763	7.8385	6.0249	5.3151	4.1821	5.2483	3.5155	0.6569	0.6192	2.6240
Yb	$f' =$	−3.8890	−4.1523	−4.8591	−5.3940	−7.2108	−0.3850	−0.3157	−2.4144	−2.9190	−1.4909
	$f'' =$	10.9742	8.2969	6.3813	5.6309	4.4329	5.5486	3.7229	0.6994	0.6592	2.7538

Table 4.2.6.8. *Dispersion corrections for forward scattering (cont.)*

Wavelength (Å)		2.748510	2.289620	1.935970	1.788965	1.540520	0.709260	0.559360	0.215947	0.209010	0.180195
Lu	$f' =$	−3.9056	−4.0630	−4.6707	−5.1360	−6.6179	−0.4720	−0.3299	−2.1535	−2.4402	−1.8184
	$f'' =$	11.5787	8.7649	6.7484	5.9574	4.6937	5.8584	3.9377	0.7436	0.7010	2.8890
Hf	$f' =$	−4.0452	−4.0564	−4.4593	−4.9466	−6.1794	−0.5830	−0.3548	−1.9785	−2.1778	−2.2909
	$f'' =$	12.2546	9.2832	7.1518	6.3150	4.9776	6.1852	4.1643	0.7905	0.7454	3.0246
Ta	$f' =$	−4.0905	−3.9860	−4.3912	−4.7389	−5.7959	−0.7052	−0.3831	−1.8534	−2.0068	−3.1639
	$f'' =$	12.9479	9.8171	7.5686	6.6850	5.2718	6.5227	4.3992	0.8392	0.7915	3.1610
W	$f' =$	−4.1530	−3.9270	−4.2486	−4.5529	−5.4734	−0.8490	−0.4201	−1.7565	−1.8819	−3.8673
	$f'' =$	13.6643	10.3696	8.0005	7.0688	5.5774	6.8722	4.6430	0.8905	0.8388	0.6433
Re	$f' =$	−4.2681	−3.9052	−4.1390	−4.4020	−5.2083	−1.0185	−0.4693	−1.6799	−1.7868	−2.8429
	$f'' =$	14.3931	10.9346	8.4435	7.4631	5.8923	7.2310	4.8944	0.9441	0.8907	0.6827
Os	$f' =$	−4.4183	−3.9016	−4.0478	−4.2711	−4.9801	−1.2165	−0.5280	−1.6170	−1.7107	−2.4688
	$f'' =$	15.1553	11.5251	8.9067	7.8753	6.2216	7.6030	5.1558	1.0001	0.9437	0.7238
Ir	$f' =$	−4.5860	−3.9049	−3.9606	−4.1463	−4.7710	−1.4442	−0.5977	−1.5648	−1.6486	−2.2499
	$f'' =$	15.9558	12.1453	9.3923	8.3074	6.5667	7.9887	5.4269	1.0589	0.9993	0.7669
Pt	$f' =$	−4.8057	−3.9435	−3.8977	−4.0461	−4.5932	−1.7033	−0.6812	−1.5228	−1.5998	−2.1036
	$f'' =$	16.7870	12.7910	9.8985	8.7578	6.9264	8.3905	5.7081	1.1193	1.0565	0.8116
Au	$f' =$	−5.0625	−3.9908	−3.8356	−3.9461	−4.4197	−2.0133	−0.7638	−1.4693	−1.5404	−1.9775
	$f'' =$	17.6400	13.4551	10.4202	9.2222	7.2980	8.8022	5.9978	1.1833	1.1171	0.8589
Hg	$f' =$	−5.4327	−4.1029	−3.8228	−3.8921	−4.2923	−2.3894	−0.8801	−1.4389	−1.5055	−1.8958
	$f'' =$	18.5241	14.1473	10.9650	9.7076	7.6849	9.2266	6.2989	1.2483	1.1796	0.9080
TI	$f' =$	−5.8163	−4.2233	−3.8103	−3.8340	−4.1627	−2.8358	−1.0117	−1.4111	−1.4740	−1.8288
	$f'' =$	19.4378	14.8643	11.5300	10.2108	8.0900	9.6688	6.6090	1.3189	1.2456	0.9594
Pb	$f' =$	−6.4779	−4.4167	−3.8519	−3.8236	−4.0753	−3.3944	−1.1676	−1.3897	−1.4497	−1.7773
	$f'' =$	20.3336	15.5987	12.1106	10.7292	8.5060	10.1111	6.9287	1.3909	1.3137	1.0127
Bi	$f' =$	−7.0419	−4.6533	−3.9228	−3.8408	−4.0111	−4.1077	−1.3494	−1.3721	−1.4290	−1.7346
	$f'' =$	21.2196	16.3448	12.7017	11.2575	8.9310	10.2566	7.2566	1.4661	1.3851	1.0685
Po	$f' =$	−7.7195	−4.9604	−4.0267	−3.8855	−3.9670	−5.1210	−1.5613	−1.3584	−1.4133	−1.7005
	$f'' =$	22.1974	17.1410	13.3329	11.8209	9.3834	11.0496	7.5986	1.5443	1.4592	1.1266
At	$f' =$	−8.5994	−5.3399	−4.1781	−3.9706	−3.9588	−7.9122	−1.8039	−1.3540	−1.4066	−1.6784
	$f'' =$	23.2213	17.9390	13.9709	12.3915	9.8433	9.9777	7.9509	1.6260	1.5367	1.1876
Rn	$f' =$	−10.2749	−5.7275	−4.3331	−4.0549	−3.9487	−8.0659	−2.0847	−1.3475	−1.3982	−1.6571
	$f'' =$	24.2613	18.7720	14.6313	12.9815	10.3181	10.4580	8.3112	1.7103	1.6167	1.2504
Fr	$f' =$	−10.8938	−6.2180	−4.5387	−4.1818	−3.9689	−7.2224	−2.4129	−1.3404	−1.3892	−1.6367
	$f'' =$	24.3041	19.6009	15.3016	13.5825	10.8038	7.7847	8.6839	1.7986	1.7004	1.3162
Ra	$f' =$	−12.3462	−6.7502	−4.7764	−4.3309	−4.0088	−6.7704	−2.8081	−1.3462	−1.3931	−1.6299
	$f'' =$	25.5374	20.4389	15.9778	14.1902	11.2969	8.1435	9.0614	1.8891	1.7863	1.3840
Ac	$f' =$	−12.3496	−7.4161	−5.0617	−4.5270	−4.0794	−6.8494	−3.2784	−1.3473	−1.3922	−1.6190
	$f'' =$	25.1363	21.3053	16.6687	14.8096	11.7994	8.5178	9.4502	1.9845	1.8770	1.4553
Th	$f' =$	−13.6049	−8.2118	−5.3692	−4.7310	−4.1491	−7.2400	−3.8533	−1.3524	−1.3955	−1.6136
	$f'' =$	26.2511	22.2248	17.4018	15.4642	12.3296	8.8979	9.8403	2.0819	1.9695	1.5284
Pa	$f' =$	−14.4639	−9.4459	−5.7337	−4.9639	−4.2473	−8.0334	−4.6067	−1.3672	−1.4083	−1.6170
	$f'' =$	27.4475	23.1548	18.1406	16.1295	12.8681	9.2807	10.2413	2.1835	2.0661	1.6047
U	$f' =$	−12.3528	−9.9362	−6.1485	−5.2392	−4.3638	−9.6767	−5.7225	−1.3792	−1.4184	−1.6188
	$f'' =$	30.1725	23.1239	18.8728	16.7952	13.4090	9.6646	10.6428	2.2876	1.1650	1.6831
Np	$f' =$	−17.4143	−11.1080	−6.6136	−5.5633	−4.5053	−11.4937	−6.9995	−1.3941	−1.4312	−1.6231
	$f'' =$	31.7405	24.1168	19.6379	17.4837	13.9666	4.1493	9.5876	2.3958	2.2679	1.7648
Pu	$f' =$	−18.0862	−11.4073	−6.9721	−5.8130	−4.6563	−9.4100	−13.5905	−1.4180	−1.4527	−1.6351
	$f'' =$	33.8963	23.2960	20.1548	17.9579	14.3729	4.3056	6.9468	2.4979	2.3652	1.8430
Am	$f' =$	−19.7042	−11.7097	−7.7881	−6.2920	−4.8483	−7.8986	−6.7022	−1.4359	−1.4684	−1.6424
	$f'' =$	37.3716	24.5715	21.1738	18.8618	15.0877	4.5125	7.3108	2.6218	2.4829	1.9358
Cm	$f' =$	−24.9307	−10.4100	−8.6102	−6.7506	−5.0611	−7.3248	−6.2891	−1.4655	−1.4952	−1.6592
	$f'' =$	41.4852	25.8115	21.8880	19.5119	15.6355	4.6980	7.6044	2.7421	2.5974	2.0271
Bk	$f' =$	−32.8492	−9.2185	−9.3381	−7.4293	−5.3481	−6.8498	−6.3438	−1.4932	−1.5203	−1.6746
	$f'' =$	32.5421	29.3028	21.9514	20.3581	16.3190	4.9086	7.9477	2.8653	2.7147	2.1208
Cf	$f' =$	−23.6520	−23.5202	−9.7799	−7.8616	−5.5545	−6.6561	−6.4144	−1.5323	−1.5562	−1.6984
	$f'' =$	21.9334	31.2999	22.4858	20.8536	16.7428	5.0785	8.1930	2.9807	2.8250	2.2102

& Fischer (1994) have extended this to the description of kinematic diffraction intensities in lattices containing anisotropic anomalous scatterers. Their treatment was developed for space groups up to orthorhombic symmetry.

All the preceeding treatments apply to scattering in the neighbourhood of an absorption edge, and to a fairly restricted class of crystals for which the local site symmetry of the electron density of states in the excited state is very different from the apparent crystal symmetry.

These approaches seek to treat the scattering from the crystal as though the scattering from each atomic position can be described by a symmetric second-rank tensor whose properties are determined by the point-group symmetries of those sites. Clearly, this procedure cannot be followed unless the structure has been solved by the usual method. The tensor approach can then be used to explain apparent deficiencies in that model such as the existence of 'forbidden' reflections, birefringence, and circular dichroism.

Scattering of X-rays from the electron spins in antiferromagnetically ordered materials can also be described by imposing a tensor description on the form factor (Blume, 1994). The tensor in this case is a fourth-rank tensor, and the strength of the interaction, even for the favourable case of resonance scattering, is several orders of magnitude lower in intensity than the polarization effects. Nevertheless, studies have been made on holmium and uranium arsenide, and significant magnetic Bragg scattering has been observed.

All the cases cited above represent exciting, state-of-the-art, scientific studies. However, none of the work will assist in the solution of crystal structures directly. Researchers should avoid the temptation, in the first instance, to ascribe anything but a scalar value to the form factor.

4.2.6.3.3.5. *Summary*

For the imaginary part of the dispersion correction $f''(\omega, \mathbf{\Delta})$, the following observations can be made.

(i) Measurements of the linear absorption coefficient μ_l from which $f''(\omega, 0)$ is deduced should follow the recommendations set out in Subsection 4.2.3.2.

(ii) There is no rational basis for preferring one set of relativistic calculations of atomic scattering cross sections over another, as Creagh & Hubbell (1987, 1990) and Kissel *et al.* (1980) have shown.

(iii) The total scattering cross section for an ensemble of atoms is not simply the sum of the individual scattering cross sections in the neighbourhood of an absorption edge and therefore $f'(\omega, 0)$ will fluctuate as $\omega \rightarrow \omega_\kappa$.

(iv) There is no dependence of $f''(\omega, \mathbf{\Delta})$ and $\mathbf{\Delta}$.

For the real part of the dispersion correction $f'(\omega, \mathbf{\Delta})$, the following observations can be made.

(i) The relativistic multipole values listed here tend to accord better with experiment than the non-relativistic and relativistic dipole values.

(ii) There is no dependence of $f'(\omega, \mathbf{\Delta})$ on $\mathbf{\Delta}$.

(iii) The theoretical tables are calculated for averaged polarizations.

(iv) Experimentalists wishing to compare their data with theoretical predictions should take account of the energy bandpass of their system when determining the appropriate theoretical value. They should also be aware of the fact that the position of the absorption edge depends on the oxidation state of the scattering atom, and that there is an inaccuracy in the tables of $f'(\omega, 0)$ of either $+0.20(E_{\rm tot}/mc^2)$ or $-0.10(E_{\rm tot}/mc^2)$.

4.2.6.4. *Table of wavelengths, energies, and linewidths used in compiling the tables of the dispersion corrections*

Table 4.2.6.7 lists the characteristic emission wavelengths that are commonly used by crystallographers in their experiments. Also included are the emission energies (since many systems use energy rather than wavelength discrimination) and the line widths (full width at half-maximum) of these lines (Agarwal, 1979; Stearns, 1984; Deutsch & Hart, 1984*a*,*b*).

4.2.6.5. *Tables of the dispersion corrections for forward scattering, averaged polarization using the relativistic multipole approach*

See Subsection 4.2.6.3 for comments on the accuracy of these tables. Note also that in the neighbourhood of absorption edges the values for condensed matter may be significantly different from the values in the tables due to XAFS and XANES effects. The values in Table 4.2.6.8 are for scattering by isolated atoms.

references